Structure, Magnetic Properties and Transport Behaviour of Layered Manganites: $La_{1.2}Sr_{1.8}Mn_{2-x}Ru_xO_7$
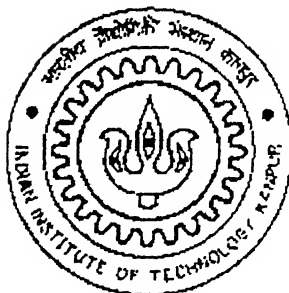
A thesis submitted
in partial fulfillment of the requirement
for the degree of

Master of Technology

by

Ruchi Singh

Materials Science Programme
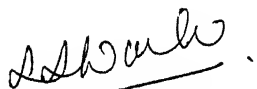*Indian Institute of Technology, Kanpur*
January, 2003

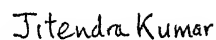A143507

CERTIFICATE

2-1-03
2.

It is certified that the work contained in this thesis entitled **"Structure, Magnetic properties and transport behaviour of layered manganites: $La_{1.2}Sr_{1.8}Mn_{2-x}Ru_xO_7$ ($0 \leq x \leq 0.2$) "** by Ruchi Singh has been carried out under my supervision and this work has not been submitted elsewhere for a degree.

(S. Sunder Manoharan)

Associate Professor

Department of Chemistry

Indian Institute of Technology,

Kanpur 208016

(Jitendra Kumar)

Professor

Materials Science Programme

Indian Institute of Technology,

Kanpur 208016

January, 2003

Acknowledgement

Abstract

Layered rare earth manganites $La_{2-2x}R_{1+2x}Mn_2O_7$ (R = Ca,Sr,Ba) , members of Ruddelsden- Popper series having general formula $A_{n+1}B_nO_{3n+1}$ (n = 2) have attracted great attention because of their applications as magnetic sensors and memory storage devices and the basic physics involved in understanding of their magnetic and electronic properties. This wide range of applications is attributed to their large magneto resistance. For application point of view, the interest is to achieve large MR ratio at low field and at high temperature. Magnetism, transport and magneto-transport in layered manganites are explained by and large within the framework of Zener's double exchange model. In this model, concentration of Mn^{3+} and Mn^{4+} play a crucial role in double exchange ferromagnetic interaction. It is realized that substitution of other 3d and 4d elements having itinerant electrons enhances the MR ratio at low magnetic field and high temperature. In our work Mn site is partially substituted by Ru, which has itinerant electron and extended d-orbital. In the work presented here, we have prepared bulk samples and thin films of Ru doped system $La_{1.2}Sr_{1.8}Mn_{2-x}Ru_xO_7$ with $0 \leq x \leq 0.2$. The series of compounds is found to be crystalline in tetragonal phase with lattice parameters increasing with Ru content up to a critical concentration x = 0.15. Ru up to 10% doping enhances the Curie temperature T_C by 55K and metal –insulator transition temperature T_P by 15K. This increased metal – insulator temperature and Curie temperature indicates that double exchange interaction enhances with increasing Ru content. In addition, no significant change in magnetoresistance (MR) is observed. At low temperatures (T < 50 K) magnetization is dominated by the spin wave excitation with a T^2 dependence, for x < 0.15 and a $T^{1.5}$ dependence is reported for $x \geq 0.15$.

CONTENTS

List of Figures

List of Tables

Rare Earth Manganites, which are known to exhibit "colossal" magneto-resistance, are widely studied over the last decade [1-5]. The interest stems from their potential technological applications in magnetic memory devices and magnetic sensor, and the fascinating physics involved. Colossal magneto-resistance (CMR) is a phenomenon involving large change in electrical resistance of the material when placed in a magnetic field. Perovskite oxides are of particular interest among this family, (namely, rare earth manganites) exhibiting CMR as well as ferromagnetic to paramagnetic transition. For viable applications, great improvements are needed in both the sensitivity and temperature dependence of the magnetoresistive response of materials. Towards this direction research is going on to explore materials, which show CMR effect at room temperature and at low magnetic fields. Apart from the CMR effect, the manganite family exhibits other interesting characteristics like electron-lattice or Jahn-Teller interaction, spin and cluster glass behavior, tunneling and powder magneto-resistance, and charge ordering.

The studies on manganites have started five decades ago by Jonker and van Santen [6,7]. They reported the existence of ferromagnetism in the mixed crystals of $LaMnO_3$-$CaMnO_3$, $LaMnO_3$ - $BaMnO_3$, and $LaMnO_3$ - $SrMnO_3$. Searle and Wang [8,9], Morrish and coworkers [10] and Leung *et al.* [11] carried out extensive investigations later on flux-grown single crystals of $La_{1-x}Pb_xMnO_3$ with $0.2 \leq x \leq 0.44$ and found metallic conductivity below the Curie temperature, T_c. The interest in manganites was revived with the experimental observation of large magneto-resistance

(MR) in thin film of $Nd_{0.5}Pb_{0.5}MnO_3$ [12], and $La_{2/3}Ba_{1/3}MnO_3$[13] $La_{0.6}Pb_{0.4}MnO_3$ [14]. MR was found to be as high as 60% at magnetic field of 5T at room temperature.

The CMR effect in manganites occurs in a small temperature regime near the Curie temperature (T_C), indicating that the electrical transport and the spin alignment are closely related. While the manganites are metallic in the low temperature regime ($T < T_C$), they are insulating at temperatures higher than T_C. It demonstrates that the transport behavior is driven by magnetism. The coexistence of metallic conductivity and ferromagnetic coupling in these materials has been explained in terms of the double exchange mechanism [15] and electron – phonon (lattice) coupling (strong enough to self trap the conduction electrons at high temperatures and to cause the localization). In addition to Double exchange and/or electron – phonon coupling, spin polarization can also be responsible for the metallic ferromagnetic state below T_C[16].

1.1 Rare earth manganites

Rare earth manganites exhibiting CMR belong to the Ruddelsden-Popper series of general formula $A_{n+1}B_nO_{3n+1}(n = 1,2,……∞)$, where A and B stand for rare earth elements La or Nd and Mn, respectively [17]. A typical CMR compound can be derived from the parent compound $LaMnO_3$ having a perovskite structure (Fig.1.1). The mixed valence oxides $La_{1-x}R_xMnO_3$ can be regarded as solid solutions of $LaMnO_3$ and $RMnO_3$, where R is a divalent ion as calcium (Ca), strontium (Sr), or Barium (Ba). These manganites of structural formula $A_{1-x}R_xMnO_3$ and perovskite structure with MnO_6 octahedra are stable only if the Goldschmidtt tolerance factor
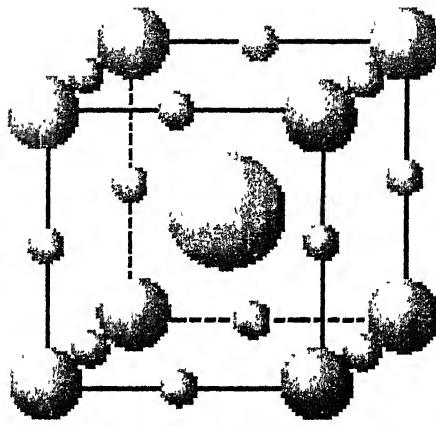
Fig.1.1: Perovskite structure

$t = (r_A + r_O)/ \sqrt{2}(r_B + r_O)$ (t > 0.8), where r_A, r_B and r_O are the radii of the rare earth element, manganese and oxygen ions, respectively. Up to finite substitution, charge balance is maintained by a fraction (x) of manganese ions assuming a tetravalent, Mn^{4+} (d^3) state. Each of the end members $AMnO_3$ and $RMnO_3$ is both antiferromagnetic and insulator [18]. The antiferromagnetic ordering is of A-type where ferromagnetically aligned layers are coupled antiferromagnetically. The insulating nature of parent compounds as well as the anisotropic magnetic interaction are related to their structure, in particular Jahn-Teller distortion around the Mn^{3+} (t_{2g}^3 e_g^1) ion. Apart from this, the ferromagnetic coupling is strongly enhanced when the e_g electron spin is parallel to the three spin - aligned t_{2g} electrons, which helps to overcome the antiferromagnetic coupling.

In $LaMnO_3$, manganese ions are in Mn^{3+} state. The five-fold degeneracy of 3d-orbital in MnO_6 octahedra splits into a two fold degenerate e_g and a three fold t_{2g} orbitals due to the crystal field of the O^{2-} ions. The ideal cubic perovskite structure is, however, distorted by cation size mismatch and the Jahn-Teller effect. The distorted structures are frequently
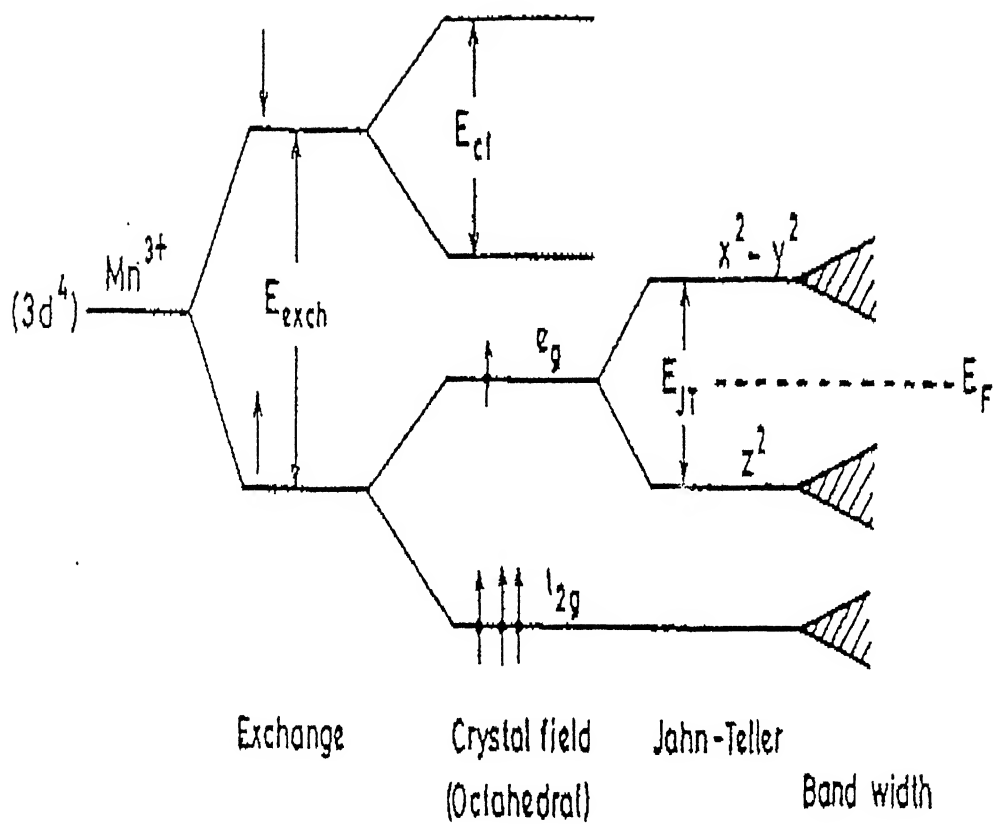
Fig.I.2: Schematic diagram of the t_{2g} and e_g orbital due to the Jahn − Teller distortion.

display orthorhombic unit cells. The Jahn-Teller effect distorts the MnO_6 octahedra in such a way that there are long and short Mn-O bonds and Mn-O-Mn bond angle deviates from 180^0. This causes a split in the e_g band (which forms the conduction band) of Mn^{3+} ions, creates a gap at the Fermi level and, makes the material insulating [19]. Schematic band diagram of $LaMnO_3$ is shown in Fig 1.2. The electronic structure ($t_{2g}^3 e_g^1$) describes the A-type antiferromagnetism via anisotropic exchange coupling.

On substituting a divalent ion at La-site, these materials display transition from a high temperature paramagnetic insulator to low temperature ferromagnetic metal with a well defined Curie temperature and metal-insulator transition temperature at a fixed x. The simultaneous observation of metallic (transport) and ferromagnetism (magnetic behavior) in manganites is explained by Zener's 'double exchange mechanism' [15]. The magnetic phase diagrams are derived on the basis of magnetic and transport studies of $La_{1-x}Ca_xMnO_3$ [2] ($0 \leq x \leq 1$) (Fig 1.3) and $La_{1-x}Sr_xMnO_3$ ($0 \leq x \leq 0.6$) [3]. The relative fraction of the double exchange and the super exchange interactions (discussed in section 1.2) control the distribution between the ferromagnetic and the antiferromagnetic phases.
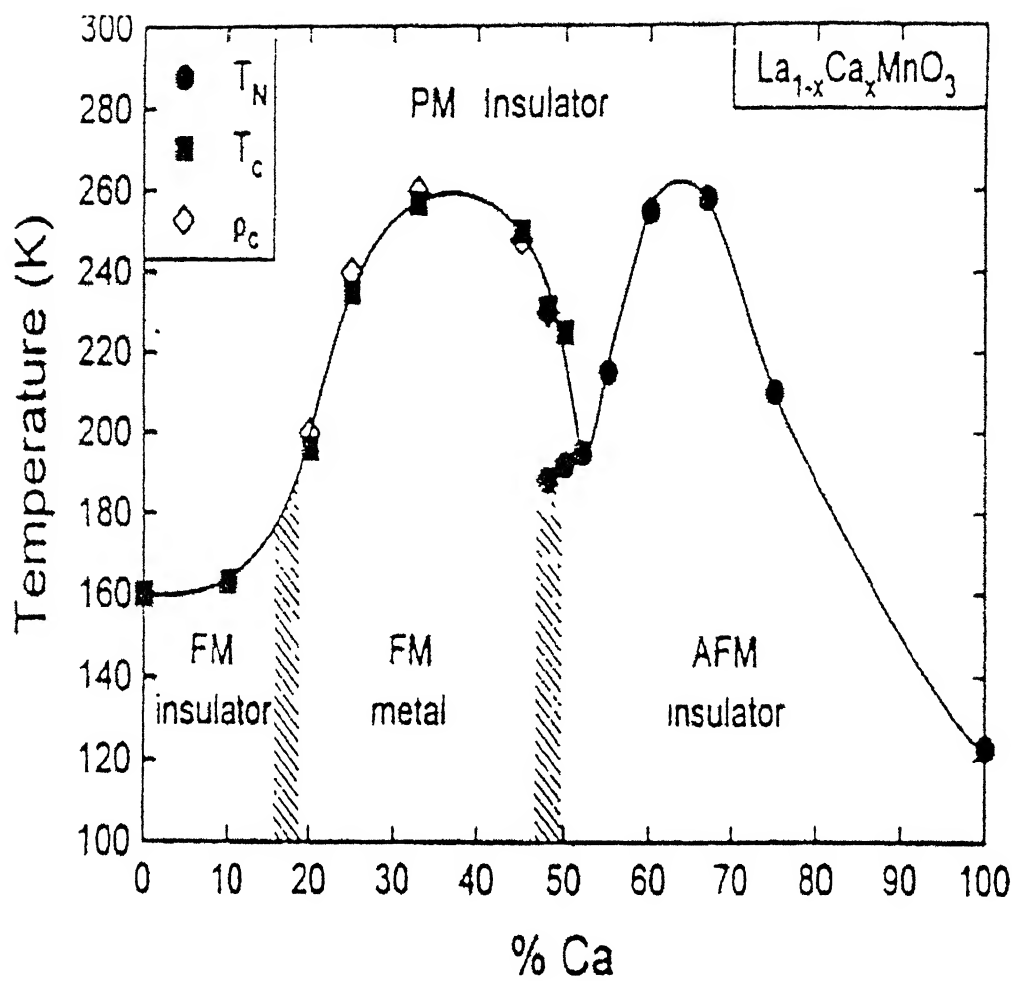
Fig-I.3 The electronic phase diagram of $La_{1-x}Ca_xMnO_3$.

1.2 Mechanisms of transport and magnetic behavior

The experimental observations of high electrical conductivity and strong ferromagnetism in manganites of composition $La_{1-x}R_xMnO_3$ with R = Ca, Sr or Ba in the range $0.2 \leq x \leq 0.4$ were first explained by Zener [15]. Accordingly, when some of La^{3+} ions are replaced by, say, divalent ions, it is necessary that a corresponding number of Mn^{3+} ions be oxidized to Mn^{4+} ions to maintain the charge neutrality. In compliance with Hund's rule, each manganese ion is in its electronic configuration of highest multiplicity, i.e., Mn^{3+} as $t_{2g}^3 e_g^1$ (s=2) and Mn^{4+} as $t_{2g}^3 e_g^0$ (s=3/2). The effective migration of Mn^{4+} ions, occurring by transfer of an electron from the neighboring Mn^{3+} ion, gives rise to high electrical conductivity. Such an electron transfer can be understood by considering the perovskite crystal structure in which O^{2-} ion lies in between two manganese ions. Now the transfer of an electron occurs from the Mn^{3+} ion to the central O^{2-} ion, simultaneously with the transfer of an electron from the central O^{2-} ion to the adjacent Mn^{4+} ion. Then Mn^{3+}-O^{2-}-Mn^{4+} state changes to Mn^{4+}-O^{2-}-Mn^{3+} state. Such a transfer is termed as a *double exchange* (Fig. 1.4). The t_{2g}^3 electrons of the Mn^{3+} ion are localized but e_g electron, which is hybridized with oxygen 2p – state, can be localized or itinerant. The lowest energy of the Mn^{3+}-O^{2-}-Mn^{4+} system corresponds to a parallel alignment of the 3d shell electron spins of the Mn^{+3} and Mn^{4+} ions. The system is inherently degenerate owing to the presence of Mn^{3+} and Mn^{4+} ions. The resulting double exchange of electron through the oxygen ion makes an indirect coupling and lowers the energy of the system with a ferromagnetic alignment of spins: thus the mechanism which is responsible for enhanced electrical conductivity also ensures a coupling leading to strong ferromagnetism.
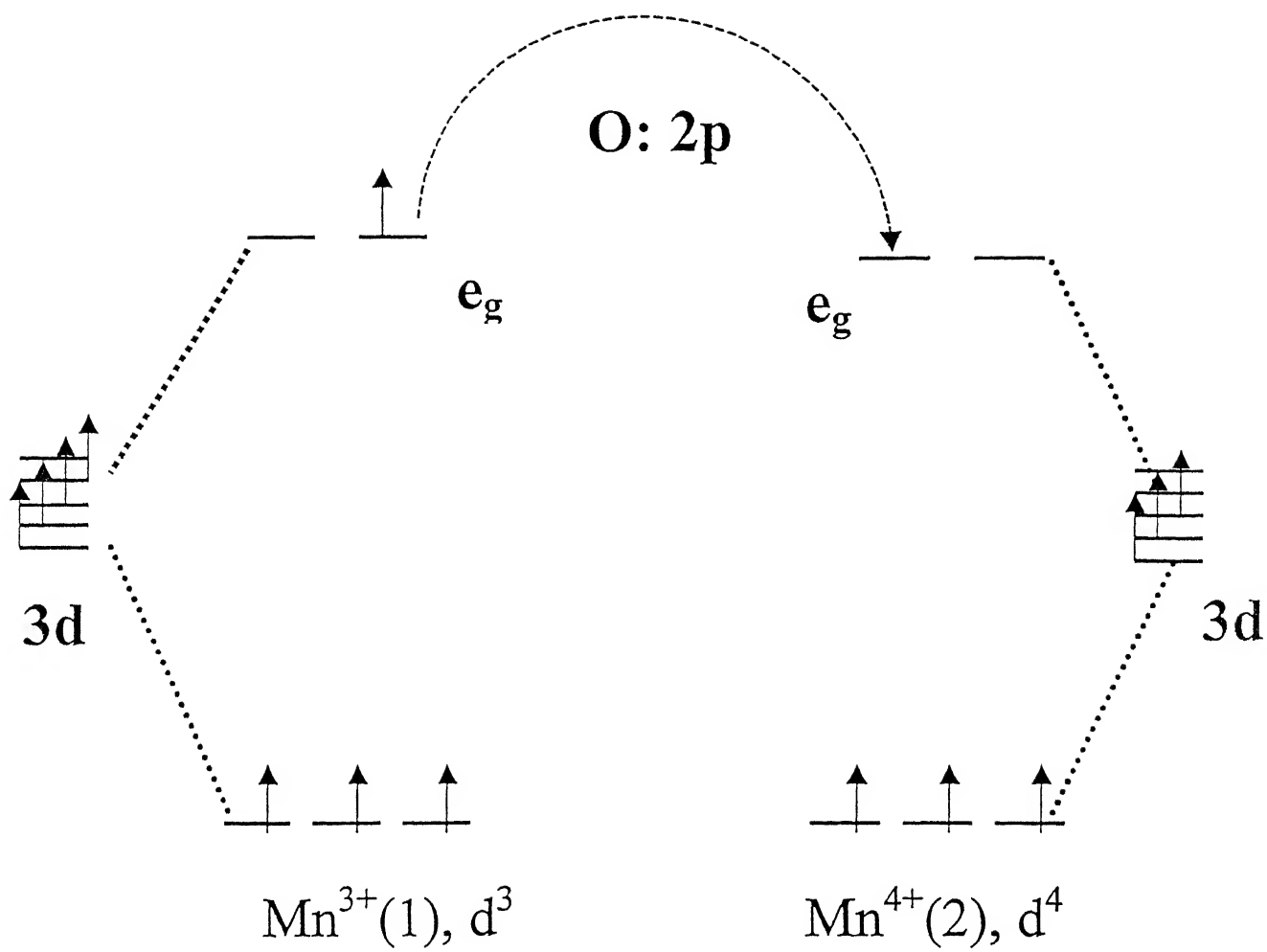
Fig.I.4: A schematic representation of the double exchange interaction.

Apart from the double exchange, a cation-anion-cation super-exchange interaction may also exist in manganites. The sign of the super-exchange interaction is predicted by the Goodenough-Kanamori-Anderson (GKA) rule [20-22]. Accordingly, while similar ions couple antiferromagnetically, different ions couple ferromagnetically. Therefore, in manganites $Mn^{3+} - O^{2-} - Mn^{3+}$ and $Mn^{4+} - O^{2-} - Mn^{4+}$ couplings should be antiferromagnetic in nature. The Hamiltonian for the super- exchange interaction is given by,

$$H = - J_{ij}\, S_i.S_j$$

where J_{ij} stands for the effective exchange integral between atoms i and j having total spins S_i and S_j and is given by

$$J_{ij} = 2b_{ij}^2 / U_{ij}$$

where U_{ij} is the Coulomb repulsive energy and b_{ij} is the transfer integral. The super-exchange energy is expressed as

$$E_s \approx - (b^2_{ij}/U_{ij})\, \cos\theta_{ij}$$

where θ_{ij} is the angle between the ith and j^{th} spins. This antiferromagnetic interaction competes with the ferromagnetic double exchange interaction and determines the magnetic phase of mixed valent manganites. In addition to GKA rules, the origin of ferromagnetism of the 3d and 4d metal based perovskites is found to be intrinsically related to the higher oxidation state of transition metal (TM) in $SrRuO_3$, $SrCoO_3$ and $CaFeO_3$ with a charge transfer gap [23]. In compound having a charge transfer gap, the lowest excited state corresponds to the electron transfer between TM ion and oxygen. An

exchange interaction between oxygen and TM spins would be much stronger than the between TM ion alone ($J_{TM-O} \sim t^2_{pd} / |\Delta|$, whereas $J_{TM-TM} \sim t^4_{pd} / |\Delta|^3$, where t_{pd} is a hybridization matrix element between TM-d and oxygen p-orbital). This gives strong tendency to the total ferromagnetic alignment of TM spins, irrespective of the sign of J_{TM-O}. Therefore, superexchange ferromagnetic interaction are observed in $Ru^{+4} - O - Ru^{+4}$, $Co^{+4} - O - Co^{+4}$ and $Fe^{+4} - O - Fe^{+4}$ [24].

The magnetic heterogeneity could arise due to the partial substitution of lanthanum and/or manganese by suitable species in the ferromagnetic $La_{1-x}A_xMnO_3$. In such cases, isolated ferromagnetic clusters may appear and, if the clusters are non-interacting, super paramagnetic phase may result [25]. If clusters interact with each other and have opposite spin alignment, a cluster-spin glass phase emerges with the net magnetization zero. There is little experimental evidence for the existence of the spin glass phase in manganites [26-28].

According to Nagaev [29], at relatively small carrier densities, if the highly conducting ferromagnetic regions are frozen as droplets inside the insulating antiferromagnetic host, the crystal as a whole continues to be an antiferromagnetic insulator at 0K. As the carrier density increases, the volume of the ferromagnetic phase increases and the droplets begin to make contact with each other forming percolative conductive paths. Further increase in carrier density leaves antiferromagnetic droplets dispersed / embedded inside the ferromagnetic host.

The parent compound, $LaMnO_3$, exhibiting a distorted cubic perovskite structure is an antiferromagnetic insulator [19]. With bivalent ion substitution at the La-site, the Mn - O -Mn distance increases and the crystal structure approaches cubic symmetry for $x \sim 0.3$ with linear Mn - O - Mn

angle as ~ 180°, leading to an increase in the electron bandwidth. In addition, substitution may also induce a decrease in the electron correlation energy and, in turn, reduce the charge transfer gap (Δ), giving rise to metallic conduction [30]. With in the framework of Zener's double exchange model, transport properties correlate with the magnetic behavior. Zener further established a quantitative relation between the electrical conductivity (σ) and ferromagnetism. Accordingly (σ) at a temperature T is given by

$$\sigma = (xe^2/ah)(T_C/T)$$

where 'x' is the fraction of the Mn^{4+} ions, a is the lattice parameter (or Mn^{3+} - Mn^{4+} separation), h is planck's constant and T_C is the Curie temperature.

Millis, Littlewood and Shraiman [31] have later on shown that double exchange interaction alone cannot completely account for the electrical resistivity data. They proposed that in addition to double exchange, a strong electron-phonon coupling arising from the Jahn-Teller distortion of the Mn^{3+} ions, called as *Jahn-Teller polaronic effect*, plays a crucial role. It, however, dominates at high temperature ($T > T_C$) and leads to magnetically disordered regime. The crossover occurs as the temperature is decreased and a metallic ferromagnetic ordered regime emerges. For this description to be valid, the root mean square displacement of oxygen ions should be large for $T > Tc$ and small for $T < Tc$. Contrary to the Jahn-Tellar polaron, the e_g carriers can be trapped by spin disorder scattering due to the local deviation of the collinear ferromagnetic ordering, resulting in the formation of the magnetic polaron in the vicinity of T_C [32,33]. Indeed, extensive theoretical studies have demonstrated that the magnetic polaron formation plays a crucial role in the paramagnetic state of the manganites [34,35]. Below T_C, magnetic

order destroys the polaron and ρ rapidly drops with decreasing temperature. The low temperature regime of the resistivity peak corresponds to the metallic conductivity, and the high temperature regime to the semiconducting / insulating state. The temperature corresponding to the maximum resistivity peak in the mixed valent manganites is commonly referred to as metal-to-insulator transition temperature, T_P and lies in the vicinity of the ferromagnetic-to-paramagnetic transition. The conduction mechanism in the paramagnetic state still remains an unresolved issue.

Viret, Ranno and Coey [36] measured electrical resistivity vs temperature characteristics of a wide range of manganite samples exhibiting metal- insulator transition and found data to follow a $T^{-1/4}$ law above T_C. They proposed that e_g electrons are localized by the random spin dependent potential (having a magnetic origin) and conduction is by variable range hopping (VRH) mechanism, assited by phonons. The resistivity (ρ) is given by [37]

$$\ln (\rho / \rho_\infty) = (T_o / T)^{1/4}$$

where ρ_∞ depends on the phonon density and the characteristic temperature T_o ($= 18\alpha^3/kN(E)$) depends on the localization length ($1/\alpha$) of the electrons and the density of states $N(E)$. Under an external magnetic field, the magnetic ordering is enhanced and the electrical resistivity decreases. The field is most effective near T_C, where the magnetic susceptibility assumes a maximum value. The large change in the resistance in the presence of an applied magnetic field is known as Colossal Magneto Resistance (CMR). The CMR ratio is defined either as $[(\rho_H - \rho_0) / \rho_0 \times 100]$ or $[(\rho_H - \rho_0)/ \rho_H \times 100]$, where ρ_H and ρ_0 are the resistivity of the material in the presence and

absence of an applied magnetic field, respectively. The main feature of the CMR effect is to show maximum resistance at temperatures close to T_C. Near T_C, electron spins of Mn^{3+}/Mn^{4+} ions get aligned by an applied magnetic field, thereby increasing the hopping probability via double exchange interaction [38]. In addition, the electron-polaron coupling becomes weaker and, in turn, increases the metallic conductivity further [39]. Analysis of the temperature and field dependence of the resistivity leads to a conclusion that resistivity depends only on the magnetization M, irrespective of whether the value is achieved by the application of a magnetic field or variation of temperature. As a result, the CMR ratio at a relatively small magnetization values is given by [2],

$$(\rho_H - \rho_0)/\rho_H = -C(x)(M/M_s)^2$$

where 'x' is the no. density of Mn^{4+} ions (or hole carrier density), M_s is the saturation magnetization and C is the Scaling constant. The value of C is ~ 4 in the vicinity of the metal - insulator boundary (i.e, $x \sim 0.17$) but decreases to ~ 1 for $x \sim 0.4$. Obviously, decrease in C with an increase in 'x' leads to an overall increase of $(\rho_H - \rho_0)/\rho_H$ ratio. Random distribution of spin directions is suppressed, decreasing thereby the average magnetic potential by the applied magnetic field or by the existing strong internal molecular field. As a consequence, the resistivity behavior of manganites with respect to an applied magnetic field and temperature can be tuned by suitably substituting ions at lanthanum and manganese sites [40,41]. This is due to the fact that the exchange interactions are sensitive to the average ionic radius of A-site and B-site cations as well as to the e_g and t_{2g} parentage of the doping elements at the B-site.

1.3 Two-dimensional (2D) layered manganites

The perovskite type structure (La, A)MnO_3 can be modified into layered structure by inserting a rock salt type layer (La,A)$_2O_2$ in between MnO_2 – sheets along c – axis which decouples the layers electrically and magnetically. Schematic structure of layered (n = 2) manganite is shown in Fig 1.5. Manganites with n = 1, $La_{2-x}A_xMnO_4$, with a layered structure are found to be 2-dimensional (2D) antiferromagnetic, i.e., single layer compound is not metallic or ferromagnetic [42], while double layer (n = 2) compound (La,A)$_3Mn_2O_7$ is found to be a ferromagnetic metal below T_C and exhibits large negative magnetoresistance [43]. In the regime, where the single layer(n=1) compound is insulating and the n = ∞ compound is metallic, the double layer has an intermediate behavior, with insulating properties above critical temperature and metallic below. With increasing n, however, the electronic and magnetic properties approach those of the n = ∞ compound. Inelastic neutron diffraction studies of the bilayered compound. reveal that the effective magnetic exchange energy between adjacent Mn ions in the (a-b) plane (in-plane) is J_{ab} = 10.3 ± 0.2 meV, which is approximately four times larger to that along c-axis (out of plane) of the bilayer, J_c = 2.5 ± 0.25 meV [44]. Due to the anisotropic exchange interaction, the resistivity along c-axis is about two orders of magnitude greater than that in the (a-b) plane [45]. The strong ferromagnetic interaction has been explained by and large within the framework of Zener's double exchange model. The ferro - para transition temperature T_C and metal – insulator transition temperature T_P for 2D layered manganite are lower than that of the 3D manganites.
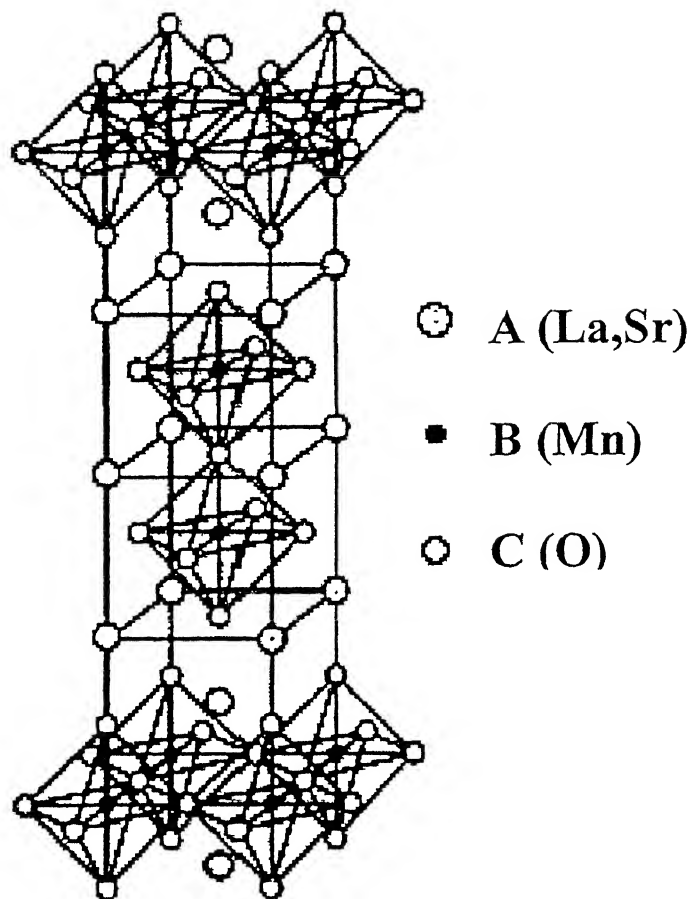
Fig.1.5: Crystal structure of double perovskite $(La,Sr)_3Mn_2O_7$

Also, the metal-insulator and magnetic transition temperatures are much different in 2D manganites in contrast to 3D manganites, where the magnetic and metal-insulator transition temperatures are nearly the same. Thus, transition temperatures (T_C and T_P) and the value of MR can be tuned in 2D layered manganites by substituting ions suitably at La and Mn sites. This is due to the fact that the exchange interactions are sensitive to Mn-O-Mn bond angle and Mn-O bond lengths.

Battle et al [46] have used neutron diffraction and synchrotron x-ray powder diffraction techniques to refine the magnetic and crystal structure of $LaSr_2Mn_2O_7$. Asano *et al* [47] have reported that $La_{2-2x}Ca_{1+2x}Mn_2O_7$ system shows two types of ferromagnetic ordering for ($0.22 \leq x \leq 0.50$). Moritomo *et al* [43] have studied the electronic and magnetic properties of the layered compound $La_{1.2}Sr_{1.8}Mn_2O_7$ and observed very large MR as compared to that of 3D, $La_{1-x}R_xMnO_3$ systems. The reduced dimensionality of the Mn-O network appears to dramatically enhance the MR effect. The enhanced MR is attained at the cost of reduced T_C. So, this trade-off relation between attaining higher T_C and lowering operating field might pose an obstacle to the development of technologically useful materials based on the layered perovskites.

Recent studies on substituted layered manganites $La_{2-2x}R_{1+2x}Mn_2O_7$ have shown interesting magnetic and transport properties [48,49,50]. Accordingly, no significant change occurs in magneto-resistance values on substitution at the manganese site, suggesting thereby that these systems are more accommodative to substitutional species than the 3-dimensional perovskites.

1.4 Effect of partial substitution of manganese in mangnites

Partial substitution of lanthanum in 3D or 2D layered manganites is important as it affects the bandwidth and influences colossal magneto resistance ratio. Similarly, partial substitution of Mn is believed to be detrimental for the electronic conduction mechanism. And controls the inter- and intra- bilayer magnetic coupling. This is illustrated below by taking some examples of Mn substitution in the rare earth manganites:

a. Chromium substitution

Cabeza *et. al.* [51] have studied $La_{0.7}Ca_{0.3}Mn_{1-x}Cr_xO_3$ to understand the effect of Cr^{3+} ($t_{2g}^3 e_g^0$) substitution, which has comparable ionic size and vacant e_g configuration of Mn^{4+} ($t_{2g}^3 e_g^0$). Here, both double exchange (DE) and super exchange (SE) mechanisms are prevalent with the former playing a greater role up to 20% substitution. For $x \geq 0.2$, a decoupling of the ferromagnetic ordering and metal-insulator transitions are observed. According to Gundakaram *et. al.* [52], the magnetic interactions between the chromium ions and adjacent manganese ions in $LaMn_{1-x}Cr_xO_3$ get mediated via the superexchange rather than the double-exchange interactions. In layered manganite $La_{1.2}A_{1.8}Mn_{2-x}Cr_xO_7$, Curie temperature T_C is found to increase slightly and then decreases with increase of chromium content (x). Also,the transport behavior reveals suppression of charge carrier itinerancy due to induced charge localization with increase in x. The transition from the ferromagnetic to a spin-glass-like state causes the magnetization to drop, along with simultaneous increase in electrical resistivity.

b. Iron substitution

Righi $et.$ $al.$ [53] found that 5% Fe-substitution of manganese in $La_{0.7}Ca_{0.3}MnO_3$ decreases the T_c by 50K and reduces the average magnetic moment measured at field of 1T by 10-15%. Pissas and coworkers [54] studied $La_{0.75}Ca_{0.25}Mn_{0.8}Fe_{0.2}O_3$ compound by Mössbauer spectroscopy and gathered evidence for the existence of ferromagnetic clusters with a size distribution. Ahn and coworkers [55] observed that the replacement of manganese by iron favors an insulating character and antiferromagnetism by opposing the effects of double exchange. Also, the electron hopping between Fe and Mn is impaired by the lack of available states in the Fe $e_{g\uparrow}$ band. The only vacant states available are in the Fe $t_{2g\downarrow}$ band, lying 2 eV above the Fe $e_{g\uparrow}$ band. This clearly indicates that electron hopping from Mn to Fe is energetically forbidden even at room temperature. Consequently, only the Mn $e_{g\uparrow}$ band is electronically active, where electron hopping can occur between Mn^{3+} and Mn^{4+} ions. Since Fe^{3+} replaces Mn^{3+}, a depletion in the Mn^{3+} / Mn^{4+} ratio occurs, thereby reducing both the population of the hopping electrons and the number of available hopping sites. This amounts to the suppression of double exchange interaction and correspondingly weakening of ferromagnetism and metallic conduction. Cai and coworkers [56] have examined the samples of $La_{0.67}Ca_{0.33}Mn_{0.9}Fe_{0.1}O_3$ and provided evidence for the existence of spin glass phase (i.e., comparison of ferromagnetic and antiferromagnetic clusters) in them. Ogale $et.al.$ [57] have studied the dependence of Fe - concentration on the properties of $La_{0.75}Ca_{0.25}Mn_{1-x}Fe_xO_3$ compounds and discovered a marked decrease in T_C at x = 0.04. Hasanain $et.al$ [58] have investigated $La_{0.65}Ca_{0.35}Mn_{1-x}Fe_xO_3$ compounds and found increased spin disorder and decrease T_C with in

creasing iron content. The resistivity data above T_P fits well with a variable range-hopping model. The rapid changes occur in T_C, magnetic moment and magnetoresistence at about 4 to 5 % Fe content. The maximum value of mangentoresistence is reported to increase consistently with 'x' and increases up to 400% for 8% iron. The results on the magnetic and transport properties of $La_{1.2}Sr_{1.8}Mn_{2-x}Fe_xO_7$ clearly indicate that the partial replacement of Mn^{3+} by Fe^{3+} ions interrupts the path of double-exchange interaction and destroys the ferromagnetic metallic state for $x \leq 0.05$.

c. Titanium substitution

Studies by Liu *et al* [59] on $La_{0.7}Ca_{0.3}Mn_{1-y}Ti_yO_3$ indicates that Ti^{4+} substitution not only creates the ferromagnetic (FM) clusters but also weakens the spin coupling between them. These variations lead to the overall decrease of the magnetization and widening of the paramagnetic-ferromagnetic transition zone. Above 10% doping, the size of the FM clusters is so small that there exists nearly no interaction between them and the compound exhibits an insulating behavior. Ti^{4+} reduces the hole carrier density and enhances the localization of the p - holes and CMR effect. Sahana and coworkers [60] have carried out a thorough study of $La_{0.6}Pb_{0.4}Mn_{0.6}Ti_{0.4}O_3$ by measuring AC magnetic susceptibility and relaxation of remanent magnetization, and provided evidence for the cluster glass formation. The magnetic and transport properties of layered manganite $La_{1.4}Sr_{1.6}Mn_{2-x}Ti_xO_7$ shows disappearance of magnetic ordering in MnO layers. Also, titanium substitution suppresses the short range 2D FM ordering and increases greatly the density of localized states. This means that the phase of titanium limits the electron transfer through the Mn^{3+}- O^{2-} - Mn^{4+} network.

d. Ruthenium substitution

Manoharan *et. al.* [14] have reported that in $La_{0.7}Sr_{0.3}Mn_{1-x}Ru_xO_3$ compounds, Ru forms mixed valence states and up to 30 % of Mn ions can be substituted by Ru with no change in crystal symmetry and with very little influence on the ferromagnetic ordering. Ranjan et al [61] have demonstrated the magnetic pair making effect between Ru and Mn ions in a variety of systems $La_{0.7}A_{0.3}Mn_{0.9}Ru_{0.1}O_3$ (A = Ca, Pb, Sr, Ba) and showed variation in T_C only by 10-30K. The aptitude of ruthenium for promoting a FM metallic state is explained on the basis of presence of both Ru^{5+} and Ru^{4+} ions which are iso-electronic to Mn^{4+} and Mn^{3+} ions, respectively [62-64]. The marginal decrease in T_C and T_P was attributed to the redox pair between Mn and Ru involving Ru^{4+} / Ru^{5+} and Mn^{3+} / Mn^{4+}. Vanitha *et. al.* [65] demonstrated influence of Ru substitution in removing charge ordering in $Nd_{0.5}Ca_{0.5}MnO_3$ system. Recently, it is observed that Ru enhances the Curie temperature ($\Delta T_C \sim 15K$) and the metal-insulator transition temperature ($\Delta T_P \sim 15K$) in bilayered manganites, $La_{1.2}Ca_{1.8}Mn_{1-x}Ru_xO_7$, where magnetism is confined to the 2-dimensional Mn-O-Mn structure [66]. Besides, mangnetoresistance ratio is found to remain largely unaffected in the vicinity of metal to insulator transition by ruthenium insertion.

1.5 Objective

Partial substitution of manganese in 2D layered manganites by other transition metal ions having itinerant electrons and extended d orbitals could affect the magnetic and electronic properties. The objective of the present work is to study the influence of partial substitution of manganese by ruthenium in polycrystalline layered manganites of the composition

$La_{1.2}Sr_{1.8}Mn_{1-x}Ru_xO_7$ (x = 0 to 0.2) on the structure, magnetic and transport properties.

1.6 Outline of the present work

1. To prepare Ru substituted $La_{1.2}Sr_{1.8}Mn_{1-x}Ru_xO_7$ sample in bulk.

2. To Characterize using X-ray diffraction.

3. To study the magnetic properties in the temperature range of 4.2K to 300K.

4. To study the transport and magnetotransport properties using four probe resistivity.

5. To make correlation between transport and magnetic behavior and to compare the behavior of these samples with $La_{1.2}Ca_{1.8}Mn_{1-x}Ru_xO_7$ series.

6. To fabricate thin film of the above sample using pulse laser deposition.

This chapter deals with various experimental aspects, which include preparation of layered manganite of composition, $La_{1.2}Sr_{1.8}Mn_{2-x}Ru_xO_7$ ($0\leq x\leq 0.2$) in bulk as well as thin films and their characterization by X-ray diffractometer, vibrating sample magnetometer and four probe resistivity.

2.1 Samples preparation

Bulk samples of manganites of composition $La_{1.2}Sr_{1.8}Mn_{2-x}Ru_xO_7$ with x = 0, 0.1, 0.15 and 0.2 were prepared by conventional solid-state reaction method. Stoichiometric amount of commercially available La_2O_3, $SrCO_3$, MnO_2, and RuO_2 (manufacturer and purity listed in Table 2.1) were mixed, ground and calcined at 1300^0C for 24 h. The product was then subjected to grinding. The resulting powders were compacted into pellets by an uniaxial hydrostatic press capable of exerting pressure of 150 kPa, and sintered in open air at 1400^0C for 24h employing a thermolyene furnace with capacity of heating up to 1700°C, and cooling rate as small as 1 C/min. This process was repeated two times in each case.

Table 2.1: Ingredients with source and purity

Materials	Manufacturer	Purity (%)
Lanthanum oxide; (La_2O_3)	Fluka	99.98
Stroncium carbonate;($SrCO_3$)	Fluka	99.00
Manganese oxide; (MnO_2)	Fluka	99.00
Ruthenium oxide; (RuO_2)	S.D. Fine Chem. Ltd.	99.00

Thin films of manganite were formed by pulse laser deposition method. Targets used were the pellets of size 12 mm diameter and 3 mm thickness produced by hydrostatic press, and sintered two times in open air at 1400^0C for 24h with intermittent grinding and pelletization. Since lattice parameter of CMR manganites match well with lanthanum aluminate ($LaAlO_3$), single crystals of $LaAlO_3$ with orientation (012) were used as substrate for the deposition of thin films. KrF eximer laser with wavelength of 248nm was used for the purpose. Irradiation of the target was carried out by an intense laser pulse of very short duration (20-30nsec) for 20 minutes. Typical energy density used to ablate the target can vary from few tens to few hundred milli Joules per mm^2. The laser beam ablates the target material which, in turn, gets deposited on the substrate held at elevated temperature (e.g., 820^0C in the present case) as shown in Fig (2.1). The substrate was mounted on the flat heater with the help of silver paste and the deposition was carried out in oxygen ambient at a pressure of 400mTorr.

Fig. 2.1: Pulse laser deposition chamber used for the deposition of thin film of composition $La_{1.2}Sr_{1.8}Mn_{2-x}Ru_xO_7$. (measured at TIFR, Mumbai)

2.2 Characterization techniques:

a) X-ray diffraction (XRD)

For phase evaluation of various manganite samples, X-ray powder diffractometer was used with a Co K_α radiation using Rich-Seifert diffractometer. The diffracted beam was received by a detector held at an angle of 2θ with the transmitted beam (θ being the angle between the sample surface and the incident beam). The X-ray tube was operated at 30kVand 20mA settings. The scanning range was set in the range 20 - 80°.

b) Magnetic Measurement

The magnetic moments of the manganites were measured with a vibrating sample magnetometer (VSM), Oxford model 3001. For this, pellets of size 3.5mmx3.5mmx1.3mm were made using a special die. The pellet was mounted in the VSM specimen holder at the end of a rigid rod attached to a mechanical resonator, which oscillates the sample at a fixed frequency. Surrounding the sample is a set of sensing coils. Applied magnetic field magnetizes the sample and with its movement, the magnetic moment alters the magnetic flux through the coils. This produces an AC voltage, which is amplified and detected using a lock- in − amplifier. By suitable processing of the signals, an output exactly proportional to the magnetic moment of the sample is obtained. Knowing the volume and mass of the sample, magnetization values can be found out. The external magnetic field is usually provided by a horizontal electromagnet. The sensitivity of VSM for the magnetic moment measurement is typically of the order of 10^{-4} emu. The schematic diagram of VSM instrument is shown in Fig 2.2. The magnetization (M) measurements were carried out in the temperature range of 4-300K at a constant magnetic field of 1 Tesla to determine the Curie temperature. Also, hysteressis plots were recorded at low temperature (5K).
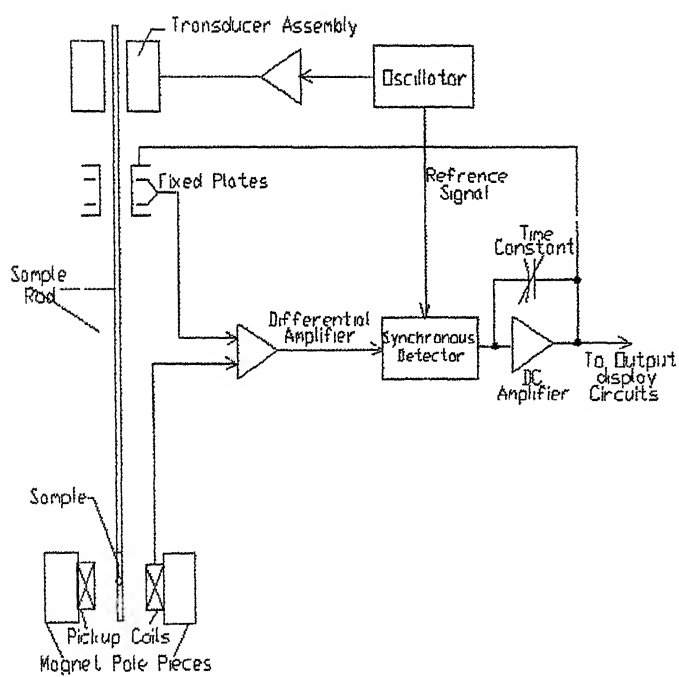
Fig.2.2: Schematic block diagram of vibrating sample magnetometer

c) Transport property measurement

The transport behavior (i.e., electrical resistivity) of manganites was determined in the temperature range 10-300K by the standard four probe method using a liquid Helium cryostat, Oxford model 2053. The four-point probe consists of two current carrying and two voltage-measuring probes. Rectangular shaped sintered pellets were used for the measurements. Contacts were made with copper wires and the silver paste. In all cases, the sample was first cooled from 300K to 10K and resistivity was recorded during the heating cycle. For the magneto-transport studies, resistivity measurements of the samples were measured similarly in the presence of a magnetic field of 7 Tesla.

3.1 Phase evolution

The X-ray diffraction patterns of bulk samples, $La_{1.2}Sr_{1.8}Mn_{2-x}Ru_xO_7$ with $0 \leq x \leq 0.2$ recorded with Co K_α radiation are shown in Figure 3.1. The 2θ values, inter-planar spacing 'd' and relative intensities of various diffraction peaks with their respective indices are given in Table 3.1-3.4. All the diffraction peaks were indexed on the basis of the $Sr_3Ti_2O_7$ - type isomorphous tetragonal structure with space group *I4/mmm*, whose standard crystal data are also included in the Tables 3.1-3.4 for comparison. The indexing of the X-ray diffraction pattern of $La_{1.2}Sr_{1.8}Mn_{2-x}Ru_xO_7$ sample with $x = 0$ suggests the tetragonal unit cell parameters as, a = 3.873 ± 0.001Å and c = 20.054 ± 0.001Å. These results agree well with the known crystal data of $La_{1.2}Sr_{1.8}Mn_2O_7$; the parameters being a = 3.87Å, c = 20.14Å for single crystal [43]. The results clearly justify the procedure undertaken for the preparation of manganites. XRD patterns of ruthenium substituted layered manganites of composition $La_{1.2}Sr_{1.8}Mn_{2-x}Ru_xO_7$ with x = 0.0, 0.1, 0.15, 0.2 first show an increase in the lattice parameters (values being a = 3.882 ± 0.001Å and c = 20.156 ± 0.001Å for x = 0.15) and then decrease for x > 0.15 (Fig. 3.2 and Table 3.5), the cell volume increases with increasing ruthenium content up to x = 0.15 at least.
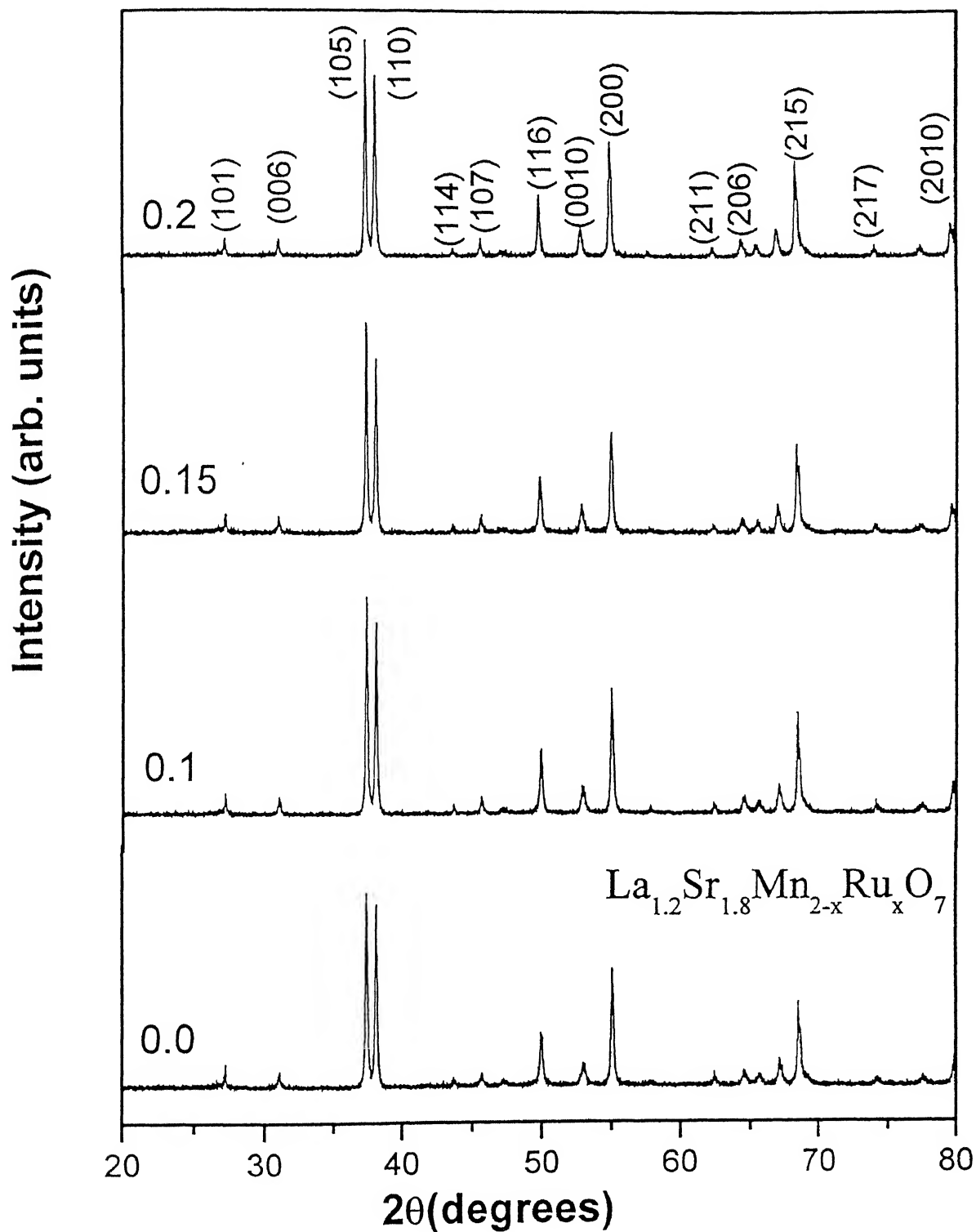
Fig 3.1: X-ray diffraction pattern of bulk polycrystalline La$_{1.2}$Sr$_{1.8}$Mn$_{2-}$
$_x$Ru$_x$O$_{7}$ (x = 0, 0.1, 0.15, 0.2) samples

Table 3.1 : 2θ, inter-planar spacing (d), relative intensity and (hkl) reflections of X-ray diffraction peaks of ruthenium substituted manganite, $La_{1.2}Sr_{1.8}Mn_{2-x}Ru_xO_7$

Standard data $Sr_3Ti_2O_7$				Observed $x = 0$			
2θ	d(Å)	Relative intensity	hkl	2θ	d(Å)	Relative intensity	hkl
26.940	3.839	10	101	27.268	3.796	13	101
30.598	3.389	10	006	31.047	3.344	10	006
36.851	2.829	100	105	37.465	2.801	100	105
37.964	2.749	60	110	38.198	2.735	94	110
43.385	2.420	5	114	43.753	2.402	6	114
45.151	2.329	2	107	45.757	2.302	8	107
46.631	2.259	2		47.305	2.231	6	
49.415	2.139	30	116	49.944	2.119	28	116
52.013	2.039	10	0010	52.974	2.006	13	0010
54.608	1.949	50	200	55.043	1.936	61	200
61.871	1.739	2	211	62.423	1.727	8	211
63.787	1.693	5	206	64.540	1.676	9	206
64.772	1.669	5	1011	65.696	1.650	7	1011
66.198	1.637	15	1110	67.131	1.618	15	1110
67.884	1.602	30	215	68.434	1.592	44	215
73.499	1.495	2	217	74.233	1.483	5	217
76.427	1.446	2	1112	77.654	1.427	6	1112
78.816	1.409	15	2010	79.837	1.394	16	2010

Table 3.2 : 2θ, inter-planar spacing (d), relative intensity and (hkl) reflections of X-ray diffraction peaks of ruthenium substituted manganite, $La_{1.2}Sr_{1.8}Mn_{2-x}Ru_xO_7$

Standard data Sr₃Ti₂O₇				Observed x = 0.1			
2θ	d(Å)	Relative intensity	hkl	2θ	d(Å)	Relative intensity	hkl
26.940	3.839	10	101	27.203	3.805	11	101
30.598	3.389	10	006	31.047	3.344	9	006
36.851	2.829	100	105	37.466	2.787	100	105
37.964	2.749	60	110	38.149	2.739	89	110
43.385	2.420	5	114	43.639	2.408	5	114
45.151	2.329	2	107	45.708	2.305	9	107
46.631	2.259	2		47.305	2.231	4	
49.415	2.139	30	116	49.944	2.119	31	116
52.013	2.039	10	0010	52.925	2.008	14	0010
54.608	1.949	50	200	54.978	1.939	58	200
61.871	1.739	2	211	62.309	1.730	6	211
63.787	1.693	5	206	64.540	1.676	9	206
64.772	1.669	5	1011	65.632	1.652	7	1011
66.198	1.637	15	1110	67.017	1.621	14	1110
67.884	1.602	30	215	68.385	1.593	47	215
73.499	1.495	2	217	74.119	1.485	7	217
76.427	1.446	2	1112	77.491	1.430	6	1112
78.816	1.409	15	2010	79.788	1.395	15	2010

Table 3.3 : 2θ, inter-planar spacing (d), relative intensity and (hkl) reflections of X-ray diffraction peaks of ruthenium substituted manganite, $La_{1.2}Sr_{1.8}Mn_{2-x}Ru_xO_7$

Standard data $Sr_3Ti_2O_7$				Observed $x = 0.15$			
2θ	d(Å)	Relative intensity	hkl	2θ	d(Å)	Relative intensity	hkl
26.940	3.839	10	101	27.203	3.805	11	101
30.598	3.389	10	006	30.933	3.356	9	006
36.851	2.829	100	105	37.335	2.796	100	105
37.964	2.749	60	110	38.085	2.743	82	110
43.385	2.420	5	114	43.591	2.411	6	114
45.151	2.329	2	107	45.643	2.307	10	107
46.631	2.259	2					
49.415	2.139	30	116	49.830	2.124	27	116
52.013	2.039	10	0010	52.811	2.012	14	0010
54.608	1.949	50	200	54.978	1.939	48	200
61.871	1.739	2	211	62.309	1.730	6	211
63.787	1.693	5	206	64.426	1.678	8	206
64.772	1.669	5	1011	65.518	1.654	8	1011
66.198	1.637	15	1110	66.507	1.624	15	1110
67.884	1.602	30	215	68.319	1.594	42	215
73.499	1.495	2	217	74.054	1.486	6	217
76.427	1.446	2	1112	77.377	1.432	5	1112
78.816	1.409	15	2010	79.674	1.397	14	2010

Table 3.4 : 2θ, inter-planar spacing (d), relative intensity and (hkl) reflections of X-ray diffraction peaks of ruthenium substituted manganite, $La_{1.2}Sr_{1.8}Mn_{2-x}Ru_xO_7$

| Standard data $Sr_3Ti_2O_7$				Observed x = 0.2			
2θ	d(Å)	Relative intensity	hkl	2θ	d(Å)	Relative intensity	hkl
26.940	3.839	10	101	27.214	4.367	9	101
30.598	3.389	10	006	30.9727	3.352	9	006
36.851	2.829	100	105	37.362	2.801	100	105
37.964	2.749	60	110	38.134	2.740	84	110
43.385	2.420	5	114	43.633	2.408	5	114
45.151	2.329	2	107	45.650	2.307	9	107
49.415	2.139	30	116	49.824	2.124	9	116
52.013	2.039	10	0010	52.811	2.012	14	0010
54.608	1.949	50	200	54.967	1.939	54	200
61.871	1.739	2	211	62.326	1.730	5	211
63.787	1.693	5	206	64.423	1.679	9	206
64.772	1.669	5	1011	65.471	1.655	7	1011
66.198	1.637	15	1110	66.915	1.626	13	1110
67.884	1.602	30	215	68.241	1.595	5	215
73.499	1.495	2	217	74.419	1.408	6	217
76.427	1.446	2	1112	77.419	1.431	6	1112
78.816	1.409	15	2010	79.654	1.399	13	2010
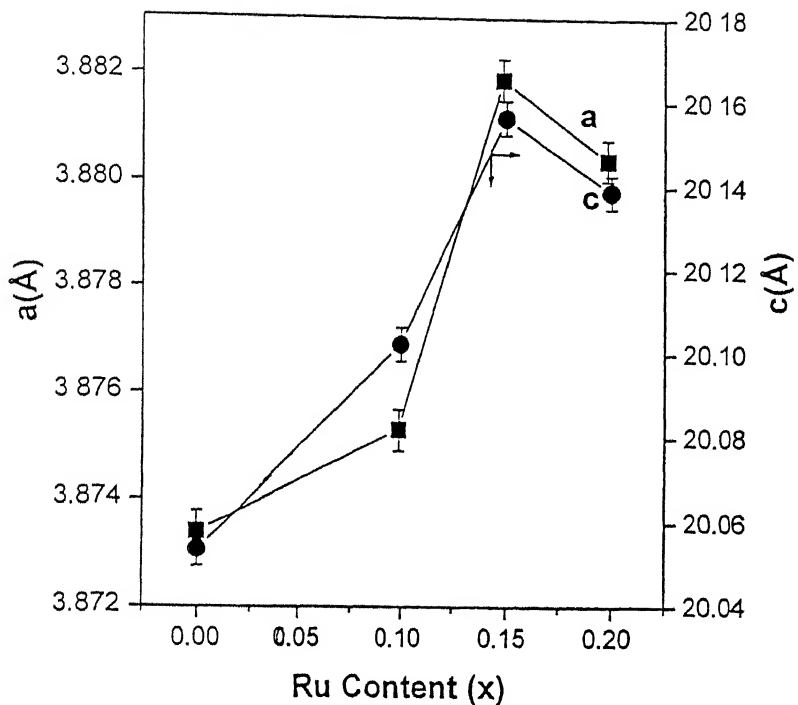
Fig 3.2 : Variation of lattice parameters 'a' and 'c' with ruthenium content (x)

Table 3.5 : Lattice parameters of various manganites $La_{1.2}Sr_{1.8}Mn_{2-x}Ru_xO_7$

Composition	a = b (Å)	c (Å)
$La_{1.2}Sr_{1.8}Mn_2O_7$	3.873	20.054
$La_{1.2}Sr_{1.8}Mn_{1.9}Ru_{0.1}O_7$	3.875	20.102
$La_{1.2}Sr_{1.8}Mn_{1.85}Ru_{0.15}O_7$	3.882	20.156
$La_{1.2}Sr_{1.8}Mn_{1.8}Ru_{0.2}O_7$	3.880	20.139

3.2 Magnetic properties

Fig.3.3a. shows the variation of magnetization as a function of temperature for the bulk samples of anisotropic manganites $La_{1.2}Sr_{1.8}Mn_{2-x}Ru_xO_7$ with x = 0.0, 0.1, 0.15, 0.2 at a fixed magnetic field of one Tesla. Clearly, the magnetization value decreases continuously with increase in temperature up to a point beyond which the change is somewhat abrupt, indicating the ferromagnetic to paramagnetic transition. Curie temperature is determined by plotting (dM/dT) vs T and identifying temperature for the maximum negative value of (dM/dT). This gives the value of the Curie temperature as 108K for the parent sample of composition $La_{1.2}Sr_{1.8}Mn_2O_7$, agreeing well with that reported earlier [43]; the value being T_C = 125K for a single crystal. Intending substitution of ruthenium causes enhancement of Curie temperature T_C by 55K for x=0.2 (Fig.3.3b) Table 3.6. Similar enhancement in Curie temperature T_C was observed earlier in ruthenium containing $La_{1.2}Ca_{1.8}Mn_{2-x}Ru_xO_7$ system by 15 K for x = 0.2 [66] and chromium substituted polycrystalline $La_{1.2}Sr_{1.8}Mn_{2-x}Cr_xO_7$ compounds [53] and attributed to an overall increase in spin magnetic moment. The increase in spin magnetic moment is due to enhanced exchange interaction as substitution of these elements the dimensionality increases.

Fig.3.4a. shows the magnetization as a function of applied magnetic field for the series $La_{1.2}Ca_{1.8}Mn_{2-x}Ru_xO_7$. The estimated saturation magnetic moment M_S = 2.63μ_B for x = 0, first increases for x = 0.1 and then decreases for x > 0.1 (Table 3.6 and Fig.3.4b). This is in sharp contrast to other elements as Cr and Fe. This suggests that Ru participates in magnetic exchange interaction.
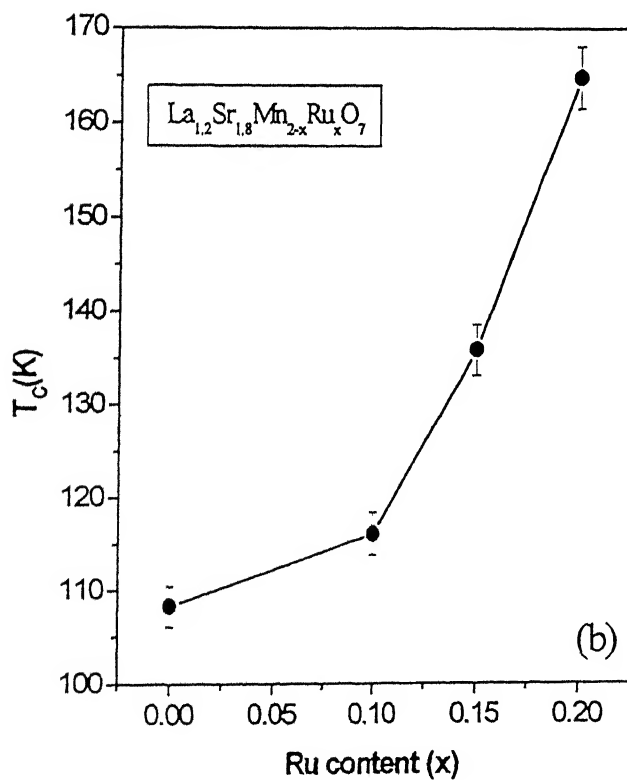
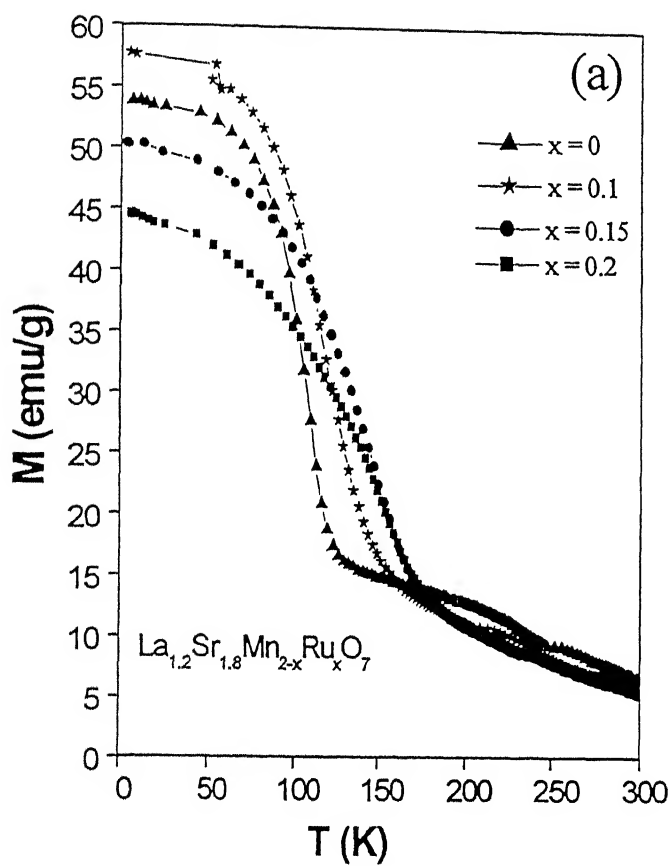Fig.3.3: (a) Plot of magnetization vs temperature of $La_{1.2}Sr_{1.8}Mn_{2-x}Ru_xO_7$
(b) Variation of T_C with Ru content (x)

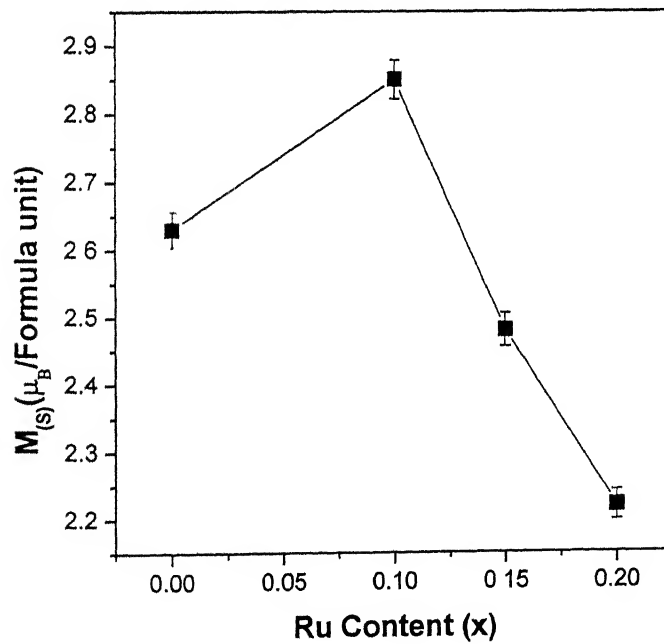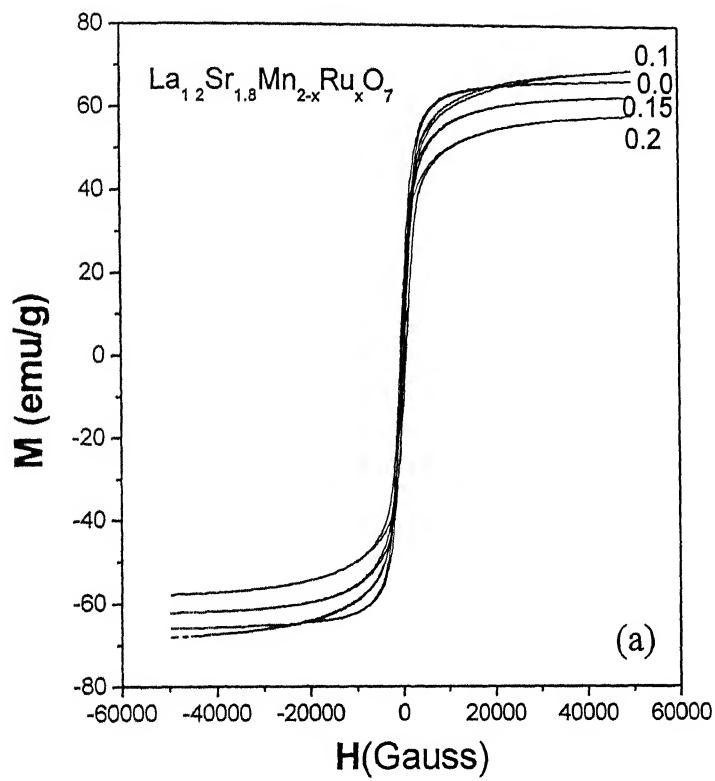**Fig.3.4**: (a) M vs. H curve for $La_{1.2}Sr_{1.8}Mn_{2-x}Ru_xO_7$
(b) Plot of saturation magnetization as a function of Ru content (x)

3.3 Transport and Magnetotransport Properties

The effect of ruthenium substitution on the transport properties of manganites $La_{1.2}Sr_{1.8}Mn_{2-x}Ru_xO_7$ is shown in Fig3.5a. The electrical resistivities versus temperature plots invariably depict metal to insulator transition at a temperature varying with the ruthenium content. The parent compound of composition $La_{1.2}Sr_{1.8}Mn_2O_7$ exhibits the transition temperature T_P as 120K. With ruthenium incorporation, T_P initially increases and assumes a value of 137K for x = 0.15, then decreases for higher ruthenium content (i.e., x = 0.2) Fig.3.5(b). The electrical resistivity plots also show a minima in low temperature regime (T < 50K) for all the compositions; the overall values, however, increase invariably with ruthenium content.

The above observations clearly demonstrate correspondence between metal to insulator and ferro- to para- magnetic transition temperatures in ruthenium substituted manganites up to a certain level, i.e., both T_P and T_C increase with x. However, beyond x=0.15, while T_C further increases up to 165K, T_P decreases sharply to ~ 102 K. The increase in transition temperatures T_C and T_P in layered manganites due to ruthenium insertion is a new result, depicting the influence of ruthenium on the magnetic ordering in such a manner so as to raise T_C and T_P values. This behaviour can be attributed largely to the formation of Ru^{4+} and Ru^{5+} states. X-ray absorption spectra of $La_{0.7}Ca_{0.3}Mn_{1-x}Ru_xO_3$ system give a clear signature for variable valency of ruthenium as Ru^{4+}/Ru^{5+}, similar to Mn^{3+}/Mn^{4+}. It is possible to envisage a redox pair such as $Mn^{3+}: Ru^{5+} \leftrightarrow Mn^{4+}: Ru^{4+}$, which accounts for the charge neutrality [61]. This is critical for the double exchange mediated coupling and initiating formation of a magnetic pair Mn/Ru. Here, the itinerant manganese e_g electrons delocalize and move to the vacant e_g orbital of Ru^{5+} ion, causing a strong double exchange mediated ferromagnetic Mn-O-Ru coupling. In addition, there exists a super - exchange ferromagnetic interaction between similar Ru^{4+} ions (due to the deloc-
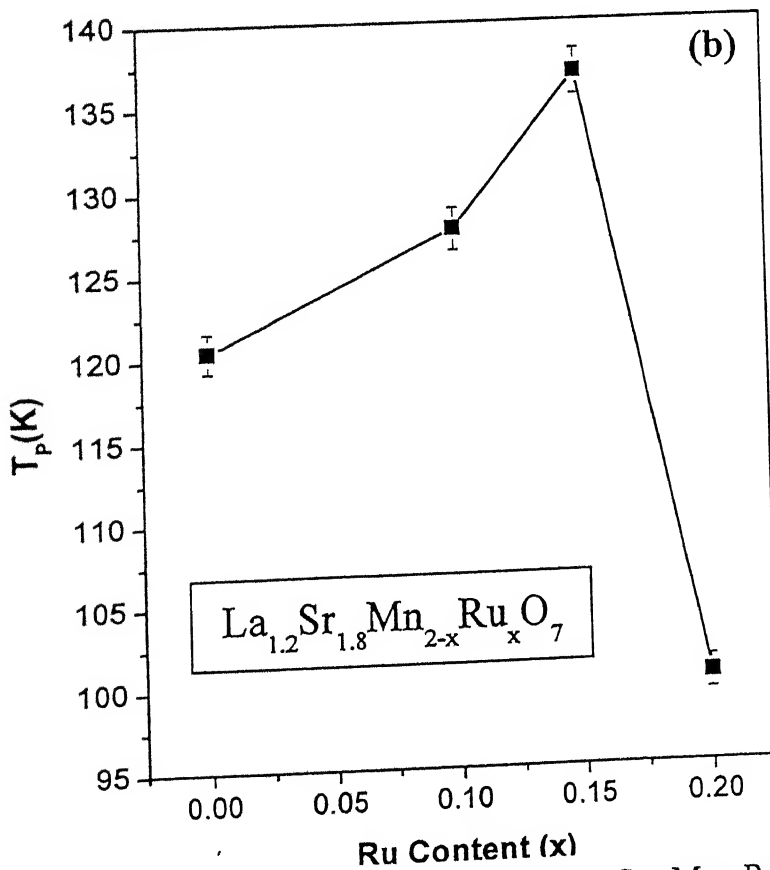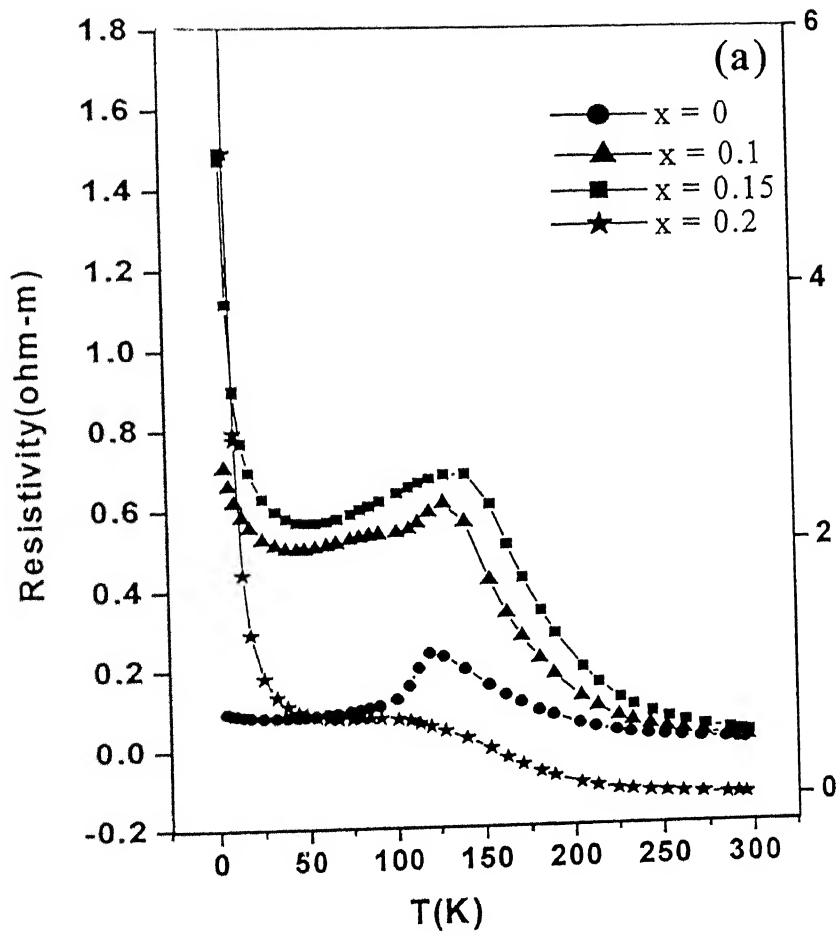
Fig. 3.5: (a) Resistivity vs temperature plots for $La_{1.2}Sr_{1.8}Mn_{2-x}Ru_xO_7$
(b) Variation of T_P with Ru content (x).

Table 3.6 : Saturation magnetization M_S, Curie temperature T_C and Metal-insulator transition temperature T_P for the series $La_{1.2}Sr_{1.8}Mn_{2-x}Ru_xO_7$

Composition	M_S (μ_B/formula unit)	T_C(K)	T_P(K)
$La_{1.2}Sr_{1.8}Mn_2O_7$	2.63	108	120
$La_{1.2}Sr_{1.8}Mn_{1.9}Ru_{0.1}O_7$	2.85	116	127
$La_{1.2}Sr_{1.8}Mn_{1.85}Ru_{0.15}O_7$	2.48	135	137
$La_{1.2}Sr_{1.8}Mn_{1.8}Ru_{0.2}O_7$	2.22	164	100

alized t_{2g} electrons) and a superexchange anti-ferromagnetic interaction between similar Mn^{4+} ions. With increase of ruthenium substitution, the ferromagnetic to anti-ferromagnetic interaction ratio varies and leads to an enhanced T_C and T_P up to critical concentration (x = 0.15). For x > 0.15, ruthenium predominantly exists in Ru^{4+} state and so reduces both the hole carrier density and the number of hoping sites. Therefore, comparing the results of $La_{1.2}Sr_{1.8}Mn_{2-x}Ru_xO_7$ and $La_{1.2}Ca_{1.8}Mn_{2-x}Ru_xO_7$ [66], we observe a large increase in T_C and T_P of $La_{1.2}Sr_{1.8}Mn_{2-x}Ru_xO_7$, which can be attributed to the ionic radii of the cation in the rock-salt layer. As the ionic radius of Sr (1.26Å) is higher than Ca (1.12 Å), the degree of mixing of the Sr:3s, O:2p and the Ru:4d orbitals is more in $La_{1.2}Sr_{1.8}Mn_{2-x}Ru_xO_7$ than $La_{1.2}Ca_{1.8}Mn_{2-x}Ru_xO_7$. Consequently, net transfer of electron density between s and d orbital increases. As Ru content in the crystal lattice increases, the carrier transfer considerably increases the charge carrier density, leading to increase in the T_C and T_P.

Fig.3.6 shows the temperature dependence of the resistance of thin film and bulk sample of $La_{1.2}Sr_{1.8}Mn_{2-x}Ru_xO_7$ (x=0.2). Both the samples correspond to semiconducting characteristics beyond a temperature (T_P), the values being 84K and 110K for thin film and bulk respectively. Notice that T_P for bulk sample is different than 102K reported before in Fig.3.5(b).The variation in T_P could be attributed to some unknown parameters or conditions prevailing during sintering with different batch of samples. However, below T_P the behaviour is somewhat different in the two cases. The resistance of thin film is invariably smaller than that of bulk sample. This can be mainly attributed to the texture nature of thin film (i.e. preferred orientation of grains, reduction in grain boundaries, better continuity etc[67].
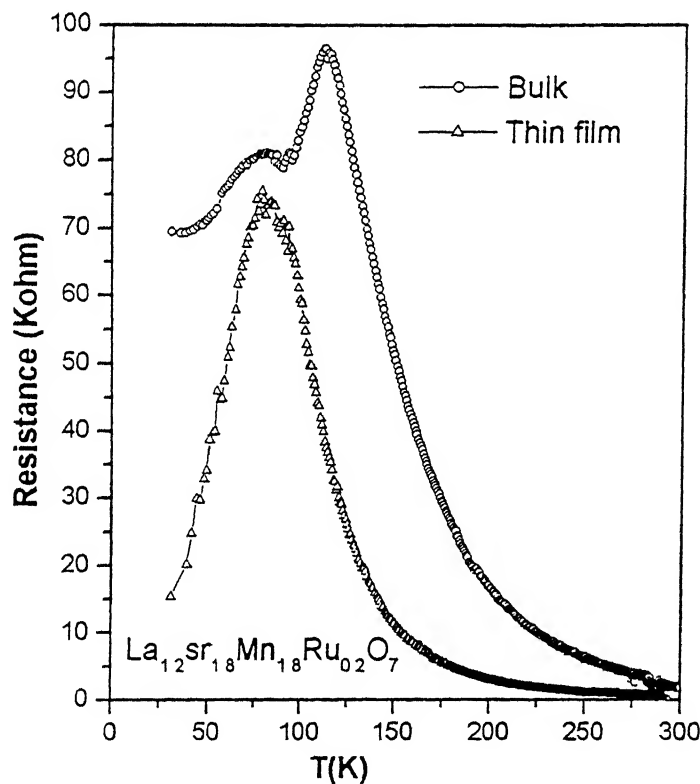

Fig.3.6. Pots of resistance vs temperature for bulk and thin film for composition $La_{1.2}Sr_{1.8}Mn_{1.8}Ru_{0.2}O_7$

For sake of comparison of the experimental results with the theoretical predictions, we plot in Fig. 3.7(a) MR = $(\rho_o - \rho_H)/\rho_o$, measured above T_C (T > $1.2T_C$), against $(M/M_s)^2$ for all the samples. The linear nature of the plots amply depict quadratic dependence of MR on the magnetization i.e. $(\rho_o - \rho_H)/\rho_o = C (M/M_s)^2$, where M and M_s are the magnetization and saturation magnetization respectively, and C is the temperature independent scaling factor, (related to the number of charge carriers 'n' per magnetic unit cell as $C \approx n^{-2/3}$) [68]. The plots of Fig. 3.7(a) allow evaluation of C from the slope and, in turn, determine the carrier density (n). The values of 'C' and 'n' are shown in Fig. 3.7(b) as a function of Ru content. The data reveal an increase in carrier density with increasing Ru content beyond x = 0.1. This increase in charge carrier density induces enhancement of both the Curie temperature and the metal-insulator transition temperature.

In Fig.3.8(a) MR vs (T/T_C) curves are shown for all the samples at 7T. These plots display the characteristics of an activated transport of spin polarons[68]. For samples with $0 \leq x \leq 0.2$ in the paramagnetic regime (T > T_C), $\rho(T)$ invariably exhibits semiconductor behaviour with a transport mechanism, best described by the Mott's variable range hopping (VRH) expression $\rho = \rho_\infty$ $\exp[(T_o/T)^{1/4}]$ [69]. Such a dependence of ρ on temperature is compatible with the existence of polarons. This is clearly evident in Fig.3.8(b) where $\ln\rho$ shows a linear dependence with $(1/T)^{1/4}$ for samples having Ru content x=0 and 0.15 at zero magnetic field. Furthermore, it can be seen that $\ln\rho$ vs $(1/T)^{1/4}$ plot obtained under a magnetic field of 7T deviates from linearity at low temperatures but continues to correspond to $(1/T)^{1/4}$ dependence at high temperatures. In fact $\ln\rho$ vs $(1/T)^{1/4}$ plot shows tendency of attaining saturation as the temperature is lowered in presence of magnetic field. Such behaviour corresponds to less pronounced activated characteristic, imply thereby that the binding energy of polarons gets reduced under the magnetic field (making clear the spin nature of
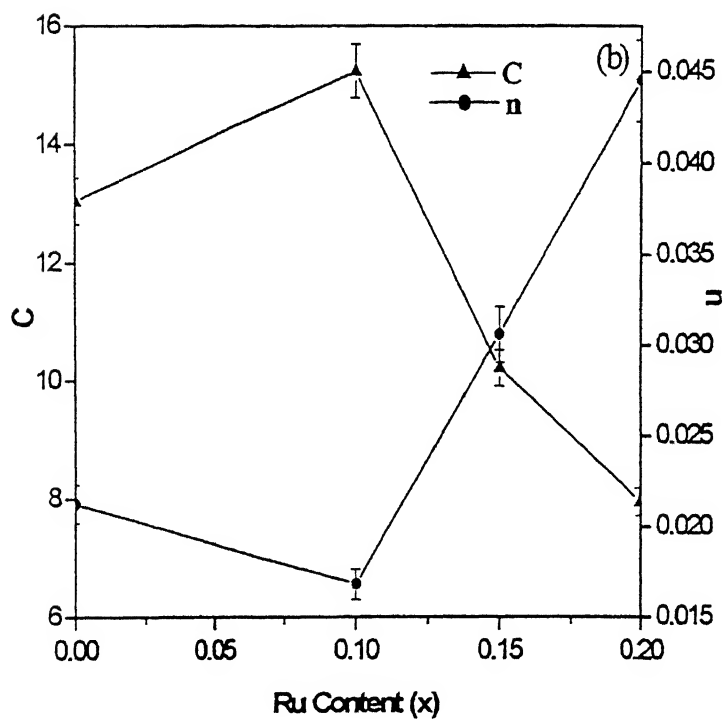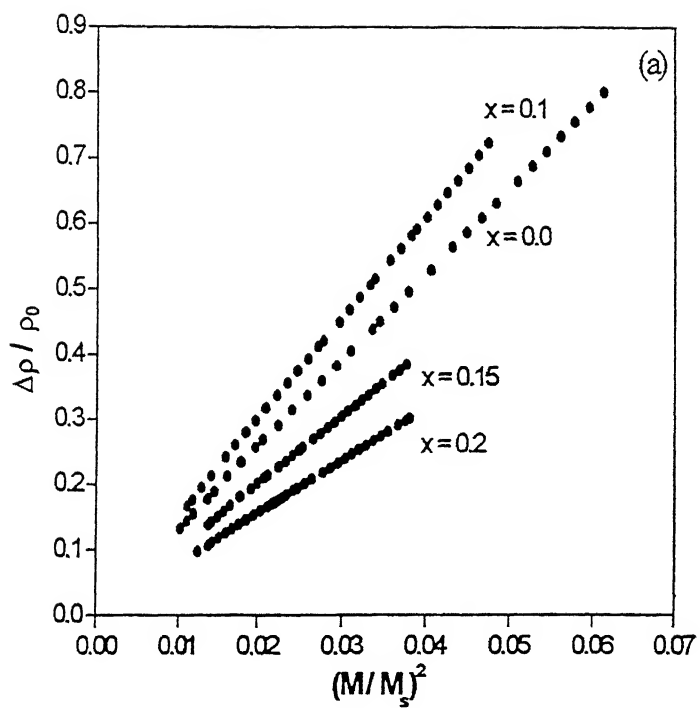
Fig.3.7: (a) Plot of $\Delta\rho/\rho_0$ vs. M/M$_s$ and (b) Plot of C and n (charge carrier density) vs. Ru content(x)
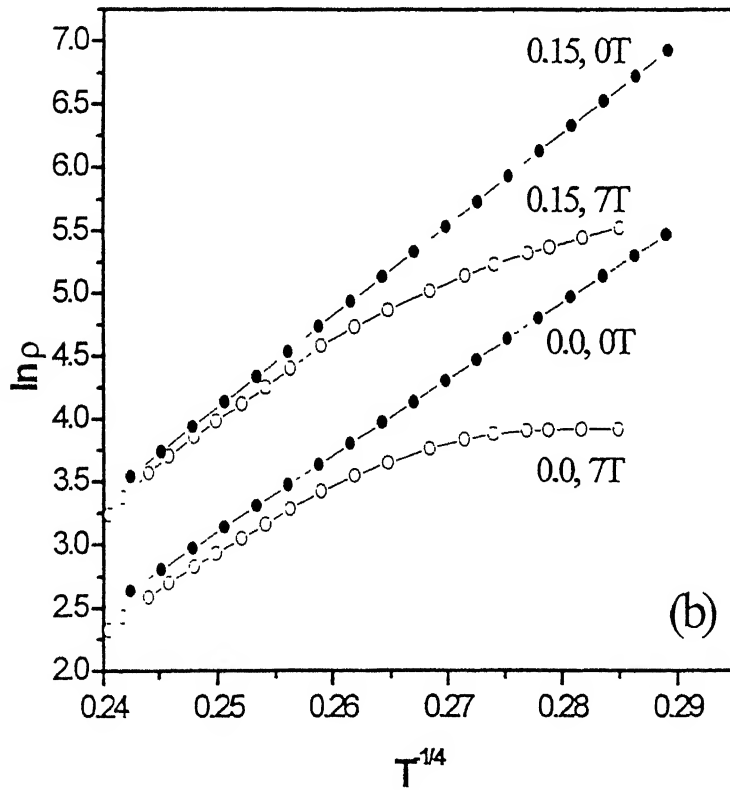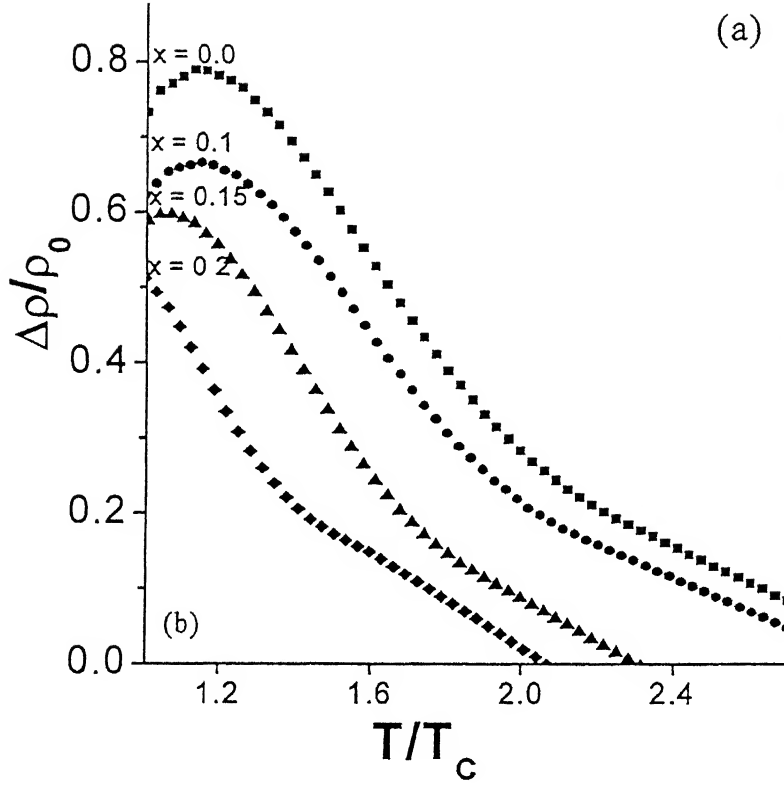
Fig.3.8: (a) Plot of $\Delta\rho / \Delta\rho_0$ vs. T/T_C and (b) Plot of $\ln\rho$ vs. $T^{-1/4}$

the polarons). The values of characteristic temperature T_o found from the slopes in the linear regime of Fig. 3.8(b) show a marginal increase with Ru substitution (e.g. $T_o = 1.3872 \times 10^7$ for $x = 0$ and $T_o = 2.82802 \times 10^7$ for $x = 0.15$), suggesting that Ru maintains the charge carrier density.

In order to understand the conduction mechanism at $T < 50K$, the resistivity $\rho(T)$ has been plotted against the temperature in Fig.3.9 (a-d). The total electrical resistivity ρ can be expressed using Matthiessen's rule as

$$\rho = \rho_o + \rho_1 T^{0.5} + \rho_2 T^n$$

where the first term ρ_o is the contribution of domain boundaries and other temperature independent scattering mechanisms, the second term ($\rho_1 T^{0.5}$) stands for weak localization and electron-electron interaction effects, and the third term ($\rho_2 T^n$) represents the resistivity due to magnetic scattering; the exponent n has been assigned values 3/2 or 4.5 for contribution arising out of electron scattering by the spin diffusive modes in ferromagnetic clusters[70] and electron-magnon interaction[71] respectively. Schiffer et al.[16] have combined all e-e, electron-phonon and electron-magnon scattering contribution in to the third term and fitted their experimental resistivity data below $0.5T_C$ with n= 2.5 as $\rho = \rho_o + \rho_1 T^{2.5}$ for $La_{1-x}Ca_xMnO_3$ system. Our resistivity data obey equation $\rho = \rho_o + \rho_1 T^{0.5} + \rho_2 T^n$ with the value of exponent 'n' as 3/2 or 2 depending upon the Ru content (Fig. 3.9). The deviation of the $\rho = \rho_o + \rho_1 T^{2.5}$ equation (which is generally used to describe the low temperature conduction mechanism for DE mediated ferromagnetic manganites) at $T < 50K$ clearly indicates that the magnetic scattering along with e-e interaction and e-phonon interaction is predominantly responsible for the resistivity. Also the value of coefficient ρ_2 increases continuously with increase in Ru content. The results suggest that the spin wave excitation effects increase with Ru insertion and dominate the magnetic scattering mechanism below 50K in the 2-D layered manganite.
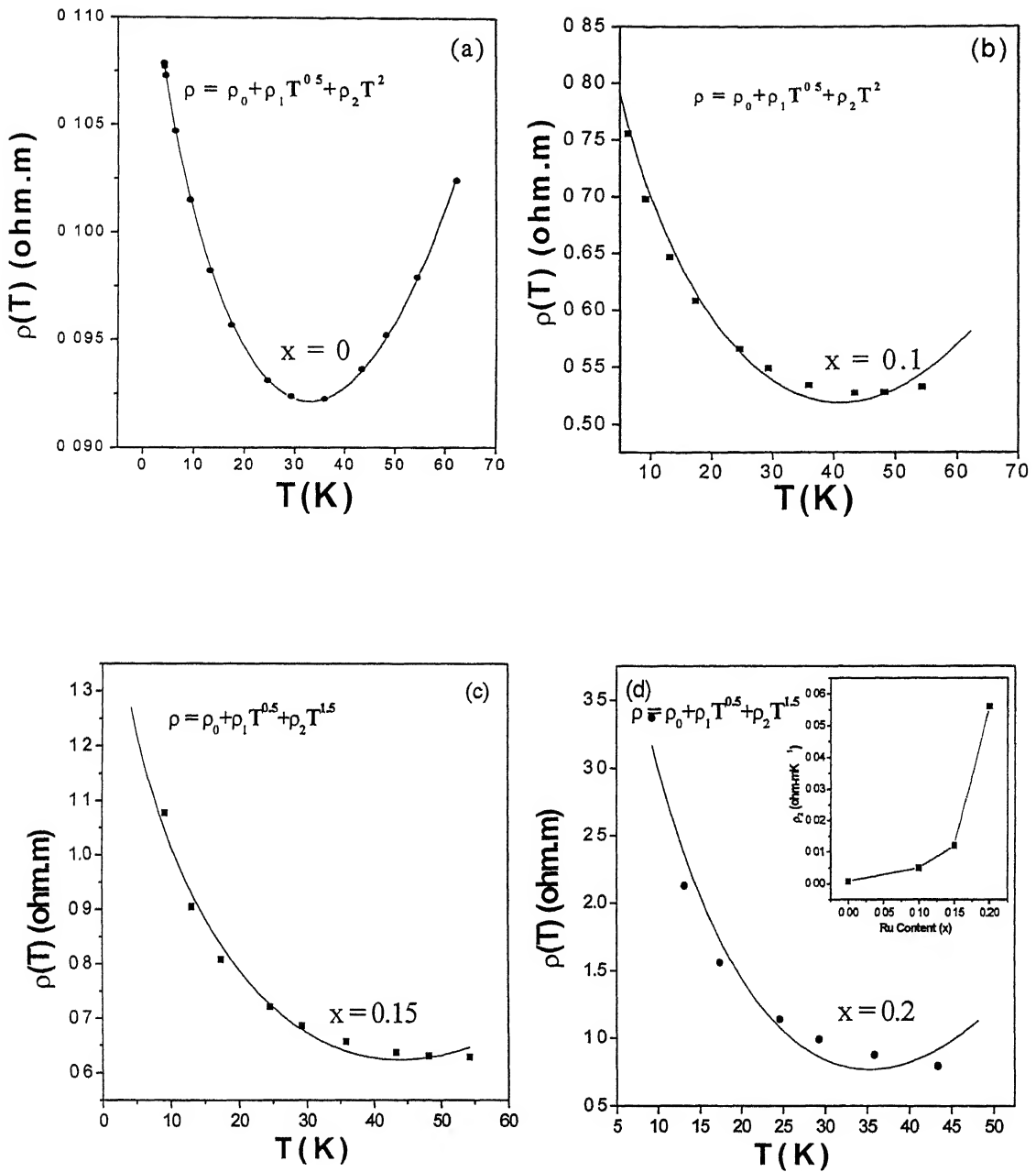
Fig.3.9: Plots of fittings of ρ (T) as a function of temperature, (a)x = 0 (b) x = 0.1
(c) x = 0.15 (d) x = 0.2 and inset of (d) Plot of ρ₂ vs. Ru content (x)

Fig.3.10 shows the temperature dependence of magnetoresistance at a field of 7T for $La_{1.2}Sr_{1.8}Mn_{2-x}Ru_xO_7$ samples with x = 0, 0.1, 0.15, and 0.2. An external magnetic field increases the magnetization and reduces the spin scattering of charge carriers. Maximum MR ratio is observed around T_P and its value is 80%, which is higher than 3D manganites (MR ratio is 60%). This enhancement in layered manganites could be due to anisotropic exchange interaction caused by the reduced dimensionality (n=2). However, the results on Ru doping indicate a strong DE interaction between the Mn and Ru ion due to magnetic pair making effect. An important feature, which is note worthy, is the 10% decrease in MR ratio in vicinity of T_P with insertion of Ru in 2D-layered manganites. Therefore, there is no significant change in the MR ratio in the vicinity of metal-insulator transition temperature.
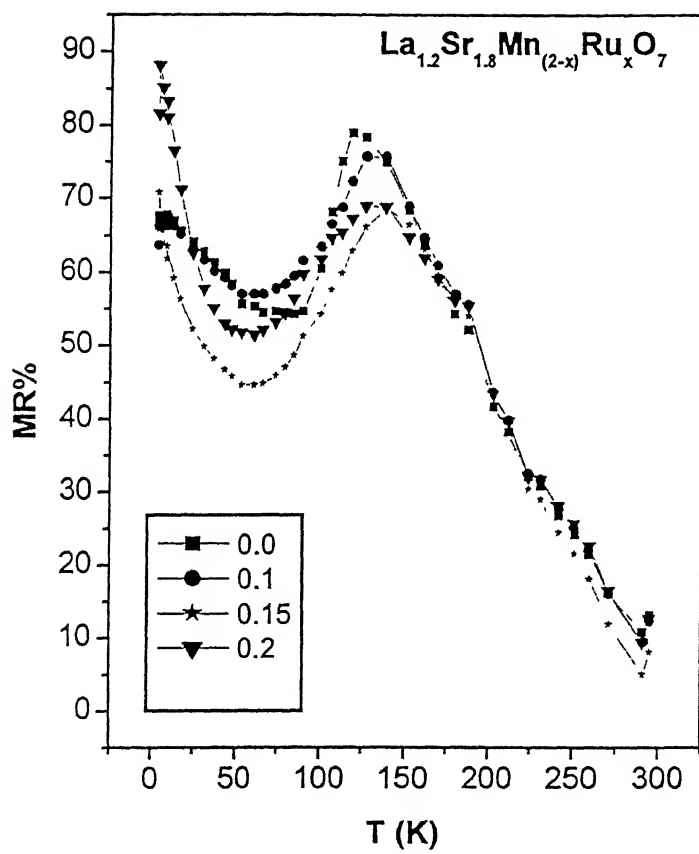
Fig.3.10: Plot of MR ratio as a function of temperature

1. A series of ruthenium substituted 2–D manganites namely, $La_{1.2}Sr_{1.8}Mn_{2-x}Ru_xO_7$ with $(0 \leq x \leq 0.2)$ has been synthesized both in bulk and thin film form.

2. The synthesized products correspond to X-ray single phase compounds, crystallizing in tetragonal structure with lattice parameters increasing with ruthenium content up to a critical concentration of $x = 0.15$. This can be attributed to the bigger ionic size of Ru^{4+} ions than the Mn^{4+}.

3. Ruthenium enhances the Curie temperature T_C by 55K and metal-insulator transition T_p by 15K for the critical concentration of $x=0.2$ This indicates the enhancement of the anisotropic double exchange interaction with increasing ruthenium content, caused by increased in the charge carrier density.

4. At temperatures below 50K, magnetization is dominated by the spin wave excitation with T^2 and $T^{1.5}$ dependence, for $x < 0.15$ and $x \geq 0.15$ respectively.

5. Ruthenium substituted manganite $La_{1.2}Sr_{1.8}Mn_{2-x}Ru_xO_7$ $(0 \leq x \leq 0.2)$ depict no significant change in magnetoresistance (MR), yet there is appreciable increase in Curie temperature T_C.

6. Pulse laser deposited thin film of $La_{1.2}Sr_{1.8}Mn_{1.8}Ru_{0.2}O_7$ exhibit lower electrical resistance than the corresponding bulk with metal-insulator transition temperature as 84K.

References

1. S. Jin, T. H. Tiefel, M. McCormack, R. R. Fastnacht, R. Ramesh, and L. h. chen, Science **264**, 413 (1994).

2. A. Urushibara, Y. Moritimo, T. Arima, A. Asamitsu, G. Kido, and Y. Tokura, Phys. Rev. B **51**, 14103 (1995).

3. P.Schiffer, A. P. Ramirez, W. Bao, and S. –W. Cheong, Phys. Rev. Lett. **75**, 3336 (1995).

4. Y. Moritimo, A. Asamitsu, and Y. Tokura, Phys. Rev. B **56**, 12190 (1997).

5. J.F. Mitchell, D. N. Argyriou, J. D. Jorgensen, D. G. Hinks, C. D. Potter, and S. D. Bader, Phys. Rev. B 55, 63 (1997).

6. G. Jonker and J. van Santen , Physica **16**, 337 (1950).

7. J. H. van Santen and G. H. Jonker, Physica **16**, 599 (1950).

8. C. W. Searle and S. T. Wang, J. Can. Phys. **47**, 2703 (1969).

9. C. W. Searle and S. T. Wang, J. Can. Phys **48**, 2023 (1970).

10. A. H. Morrish, B. J. Evans, J. A. Eaton, and L. K. Leung, J. Can. Phys. **47**, 1969 (1969).

11. L. K. Leung, A. H. Morrish and C. W. Searle, J. Can. Phys. **47**, 2697 (1969).

12. R. M. Kusters, J. Singleton, D. A. Keen, R. McGreevy and W. Hayes, Physica B **155**, 362 (1989).

13. R. von Helmholt, J. Wecker, B. Holzapfel, L. Schultz and K. Samwer, Phys. Rev. Lett. **71**, 2331 (1993).

14. S. Sundar Manoharan, N. Y. Vasanthachanya, M. S. Hegde, K. M. Satyalakshmi, V. Prasad, and S. V. Subramanyam J. Appl. Phys. **76**, 3923 (1994).

15. C. Zener, Phys. Rev. **82**, 403 (1951). *ibid* **81**, 440 (1951).

16. P.Shiffer, A.P.Ramirez, W. Bao and S.-W.Cheong, Phys. Rev. Lett. **75**, 336 (1995).

17. S. N. Ruddlesden and P. Popper, Acta Crystallogr. **11**, 541 (1958).

18. E. O. Wollan and W. C. Koehler, Phys. Rev. **100**, 545 1955).

19. S. Satpathy, Z. S. Popovic, and F. R. Vukajlovic, J. Appl. Phys. **79**, 4555 (1996).

20. J. B. Goodenough, Phys. Rev. **100**, 564 (1955); J. Phys. Chem. Solids 6, 287 (1958).

21. J. Kanamori, J. Phys. Chem. Solids, **10**, 87 (1959).

22. P. W. Anderson, Phys. Rev. **115**, 2 (1959).

23. J. B. Goodenough, *Magnetism and the Chemical Bond*, John Wiley & Sons, New York, London, 1963.

24. D. I. Khomskii and G. A. Sawatzky, Solid State. Comm. **102**, 87 (1997).

25. J. A. Mydosh, Spin glasses: An experimental introduction, Taylor & Francis, London, Washinton, DC (1993).

26. J. M. De Teresa, M. R. Ibarra, J. Garcia, J. Blasco, C. Ritter, P. A. Algarabel, C. Marquina, and del Moral, Phys. Rev. Lett. **76**, 3392 (1996).

27. J. Blasco, J. Garcia, J. M. de Teresa, M. R. Ibarra, J. Perez, P. A. Algarabel, C. Marquina, Phys. Rev. **B, 55,** 8905 (1997).

28. P. Raychaudhuri, T. K. Nath, P. Sinha, C. Mitra, A. K. Nigam, S. K. Dhar and R. Pinto, J. Phys.: Condens. Matter **9,** 10919 (1997).

29. E. L. Nagaev, Physics-Uspekhi, **39,** 781 (1996).

30. H. L. Ju, H. –C. Sohn and K. M. Krishnan, Phys. Rev. Lett. **79,** 3230 (1997).

31. A. J. Milli, P. B. littlewood and B. I. Shrayman, Phys. Rev. Lett. **74,** 5144 (1995)

32. Furukawa, J. Phys. Soc. Jpn. **63,** 3214 (1994); **64,** 3164 (1995).

33. C. M. Varma, Phys. Rev. B **54,** 7328 (1996).

34. P. Horsch, J. Jaklic and I. Mack, Phys. Rev. B **59,** R14149 (1999).

35. Batisa, J. Eroles, M. Avignon and B. Alascio, Phys. Rev. B **58,** R14689 (1998).

36. M. Viret, L. Ranoo, and J.M.D. Coey, Phys. Rev. B **55,** 8067 (1997)

37. R. von Helmholt, L. Haupt, K. Barner and U. Sondermann, Solid State Comm. **82,** 693 (1992).

38. J. Inoue, J. Phys. D: Appl. Phys. **31,** 643 (1998).

39. A. J. Millis, J. Appl. Phys. **81,** 5502 (1997).

40. R. Mahendiran, R. Mahesh, A. K. Raychaudhuri and C. N. R. Rao. Phys. Rev. B **53,** 12160 (1996).

41. H. Y. Hwang, S. –W. Cheong, P. G. Radaelli, M. Marezio, B. Batlogg, Phys. Rev. Lett. **75,** 914 (1995).

42. Y. Moritomo, Y. Tomioka, A. Asamistu. Y. Tokura and Y.Matsui. Phys. Rev. B **51,** 3297 (1995).

43. Y. Moritomo, A.Asamitsu, H.Kuwahara and Y. Tokura, Nature **380,** 141, (1996).

44. T. Chatterji, L. P. Regnault, P. Thalmeier, R. Suryanarayanam, G. Dhalenne, and A. Rcvcolevschi, Phys. Rev. B **60.** R6965 (1999).

45. J. F. Mitchell, D. N. Argyriou, J. D. Jorgensen, D. G. Hinks, C. D. Potter, and S. D. Bader, Phys. Rev. B **55,** 63 (1997).

46. P. D. Battle, M. A. Green, N. S. Lasky, J. E. Millbum, P. G. Radaelli, M. J. Rosseinsky,

S. P. Sullivan, and J.F. Vente, Phys. Rev. B **54**, 15967 (1996).

47. H. Asano, J. Hayakawa, and M. Matsui, Phys. Rev. B **56**, 5395 (1997).

48. Ting Yu, Wenhai Song, Kaiyou Wang, Shouguo Wang, and Yuping Sun, Phys. Stat. Sol. (a) **172**. 451 (1999).

49. Hong Zhu, SunTan, Wei Tong and Yu Heng Zhang, Appl. Phys. Lett. 80, 3778 (2002).

50. N.O. Moreno, P.G.Pagliuso, C.Rettori, J.S.Gardner, J.L.Sarrao, J.D.Thompson, D.L.Huber, A.Garcia – Flores and S.B.Oseroff, Physica B **292**, 1 (2000).

51. O. Cabeza, M. Long, C. Sevevac, M. A. Bari, C. M. Muirhead, M. G, Francesconi and Greaves, J. Phys. Condens. Matter. 11, 2569 (1999).

52. R. Gundakaram, A. Arulraj, P. V. Vanitha, C. N. R. Rao, N. Gayathri, A. K. Raychaudhuri and A. K. Cheetham, J. Solid State Chem. 127, 354 (1996).

53. L. Righi, P. Gorria, M. Insausti, J. Gutierrez and J. M. Barandiran, J. Appl. Phys. **81**, 5767 (1997).

54. M. Pissas, G. Kallias, E. Devlin, A. Simopolous and D. Niarchos, J. Appl. Phys. **81**, 5770 (1997).

55. K. H. Ahn, X. W. Wu, K. Liu and C. L. Chien, Phys. Rev. B **54**, 15299 (1996).

56. J. Cai, C. Wong, B. Shen, J. Zhao and W. Zhan, Appl. Phys. Lett. **71**, 1727 (1997).

57. S. B. Ogale, R. Shreekala, R. Bathe, S. K. Date, S. I. Patil, B. Hannoyer, F. Petit and G. Marest, Phys. Rev. B **57**, 7841 (1998).

58. S. K. Hasanain, M.Nadeem, W. H. Shah, M. J. Akhtar, and M. M. Hassan. J. Phys.: Condens. Matter **12**, 9007 (2000).

59. Liu, X. Xu and Y. Zhang, Phys. Rev. B **62**, 15112 (2000).

60. M. Sahana, K. Dörr, M. Dörr, D. Eckert, K. –H. Müller, K. Nenkov, L. Schultz, M. S. Hegde, J. Magn. Magn. Mater. **213**, 253 (2000).

61. Ranjan K. Sahu and S.Sundar Manoharan, Appl. Phys.Lett. **77**, 2382 (2000).

62. S.Sundar Manoharan, Ranjan K. Sahu, Manju L. Rao, D.Elefant and C.M. Scheneider, Euro. Phys. Lett. **59**, 451 (2002).

63. Ranjan K. Sahu, Z.Hu, Manju L. Rao, S.Sundar Manoharan, T. Schmidt, B. Richter, M. Knupfer, M.Golden, J. Fink and C.M. Scheneider, Phys. Rev. B. **66**, 1444 (2002).

64. Ranjan K. Sahu and S. Sundar Manoharan, J. Appl. Phys. 91, 1 (2002).

65. P. V. Vanitha, P.N. Santosh, R.S. Singh, C. N. Rao, and J. P. Attfield, Phys. Rev. B **59**, 13539 (1999).

66. Ranjan K. Sahu, Qureshi Mohammad, Manju L. Rao, and S.Sundar Manoharan, Appl. Phys. Lett. **80**, 88 (2002).

67. H. Asano, J. Hayakawa and M. Matsui, Appl. Phys. Lett. **70**, 2303 (1997).

68. P. Majumdar and P. Littlewood, Phys. Rev. Lett. **81**, 1314 (1998); Nature **395**, 479 (1998).

69   Sir Nevill Mott, Conduction in Non-crystalline Materials (Clarendan Press, Oxford, (1993), P. 17ff.

70. N. Rivier and J. Adkins, J. Phys. F **5**, 1745 (1975).

71. K. Kubo and N. Ohata, J. Phys. Soc. , Japan, **33,** 21 (1972).

Publications arising out of this work

1. S. Sundar Manoharan, Ruchi Singh, R. K. Sahu, Jitendra Kumar, D. Elefant and C. M. Schneider "Large increase in ferromagnetic and metal-insulator transition from inter plane interaction in $La_{1.2}Sr_{1.8}Mn_{2-x}Ru_xO_7$ layered manganite" , J. Phys: Conden. Matter (Accepted)

2. S. Sundar Manoharan, Ruchi Singh, Brajendra Singh, Jitendra Kumar, S.P.Pai, and A.K.Nigam, "Transport and magnetism in pulsed laser deposition of $La_{1.2}Sr_{1.8}Mn_{2-x}Ru_xO_7$ thin films" App.Phys Lett. (to be communicated)